

Review

# Virtual Inertia: Current Trends and Future Directions

Ujjwol Tamrakar <sup>1</sup>, Dipesh Shrestha <sup>1</sup>, Manisha Maharjan <sup>1</sup>, Bishnu P. Bhattarai <sup>2</sup>,  
Timothy M. Hansen <sup>1</sup> and Reinaldo Tonkoski <sup>1,\*</sup>

<sup>1</sup> Department of Electrical Engineering and Computer Science, South Dakota State University, Brookings, SD 57007, USA; ujjwol.tamrakar@jacks.sdstate.edu (U.T.); dipesh.shrestha@jacks.sdstate.edu (D.S.); manisha.maharjan@jacks.sdstate.edu (M.M.); timothy.hansen@sdstate.edu (T.M.H.)

<sup>2</sup> Department of Power and Energy Systems, Idaho National Laboratory, Idaho Falls, ID 83415, USA; bishnu.bhattarai@inl.gov

\* Correspondence: reinaldo.tonkoski@sdstate.edu; Tel.: +1-605-688-6298

Received: 30 April 2017; Accepted: 19 June 2017; Published: 26 June 2017

**Abstract:** The modern power system is progressing from a synchronous machine-based system towards an inverter-dominated system, with large-scale penetration of renewable energy sources (RESs) like wind and photovoltaics. RES units today represent a major share of the generation, and the traditional approach of integrating them as grid following units can lead to frequency instability. Many researchers have pointed towards using inverters with virtual inertia control algorithms so that they appear as synchronous generators to the grid, maintaining and enhancing system stability. This paper presents a literature review of the current state-of-the-art of virtual inertia implementation techniques, and explores potential research directions and challenges. The major virtual inertia topologies are compared and classified. Through literature review and simulations of some selected topologies it has been shown that similar inertial response can be achieved by relating the parameters of these topologies through time constants and inertia constants, although the exact frequency dynamics may vary slightly. The suitability of a topology depends on system control architecture and desired level of detail in replication of the dynamics of synchronous generators. A discussion on the challenges and research directions points out several research needs, especially for systems level integration of virtual inertia systems.

**Keywords:** frequency stability; microgrid control; renewable energy; virtual inertia

---

## 1. Introduction

The demand for clean energy in the modern power system is on the rise, driven by factors such as fuel prices, laws, and regulations. Renewable energy sources (RESs) like photovoltaic (PV) and wind energy are now gradually starting to dominate the energy generation mix, replacing traditional generation sources, such as coal and nuclear [1,2]. The popularity of distributed PV plants further escalates the penetration of renewables in the modern power system. The global installation of wind and PV generation exceeded 400 GW and 200 GW, respectively, by the end of 2015 [3]. Countries like Ireland and Germany already have annual RES penetrations of more than 20% [4]. In Denmark, wind power alone has the capacity to meet 40% of the country's instantaneous electricity demand, which is the highest among all the countries. The rapid development of RES is causing the modern power grid to gravitate towards an inverter-dominated system from a rotational generator-dominated system, as illustrated in Figure 1. PV systems and most modern wind turbines are interfaced through inverters. Although this is advantageous from the point-of-view of harvesting RES, the inverter-based generation does not provide any mechanical inertial response, and hence compromises frequency stability [4–6].

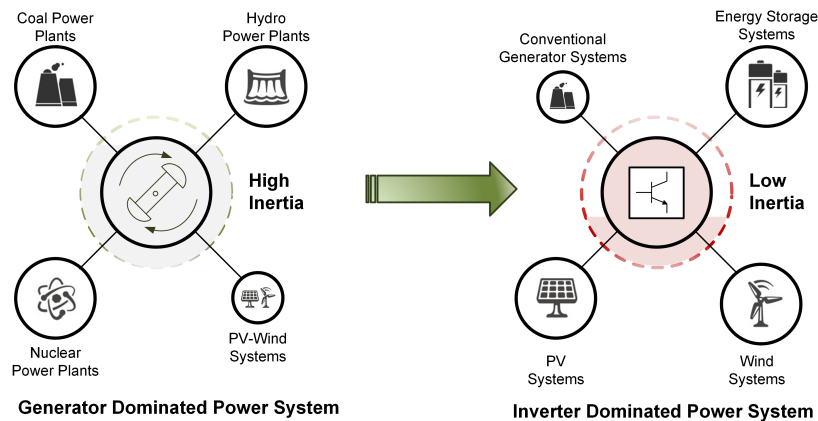


**Figure 1.** Evolution towards an inverter dominated power system.

Recent reports and studies have shown frequency stability to be a matter of significant concern due to lack of inertial response from RESs. The independent system operator, Electricity Reliability Council of Texas (ERCOT) has reported a continuous decline in the inertial response of its system and recommends additional inertial response [7,8]. Figure 2 illustrates the change in frequency in the ERCOT interconnection for two time periods for the same amount of generation loss. The change in frequency per generation loss is increasing yearly, and this trend is highly correlated with increased RES penetration over the same time-period. Similarly, the European Network of Transmission System Operators for Electricity (ENTSO-E) has reported increased frequency violations in the Nordic grid correlated with increased RES penetration [9]. As a consequence, inertial response from wind turbines is now mandatory in many countries [10,11] and the trend is extending towards PV plants as well. Accordingly, there is a strong practical relevance to research on virtual inertia systems which was of an academic nature in the past.

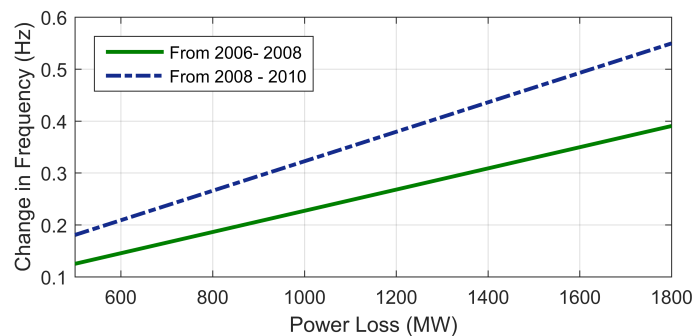


**Figure 2.** Increase in frequency changes in Electricity Reliability Council of Texas (ERCOT) connection due to generation loss [7].

In order to maintain the power generation and load balance, various control actions are implemented in a power system over multiple time-frames as illustrated in Figure 3. The governor response is the primary control action which takes place within the first few seconds (typically 10–30 s) of a frequency event and aims at reducing the frequency deviation. The automatic generation control is the secondary control action which takes place within minutes (typically 10–30 min) and restores the system frequency back to the nominal value. The tertiary control action is the reserve deployment when actions are taken to get the resources in place to handle present or future disturbances in the system. Whenever there is an imbalance between the generation and consumption in a power system, the generators cannot respond instantaneously to balance the system. The kinetic energy stored in the rotors is responsible for counteracting this imbalance through inertial response until the primary

frequency control has been activated. As conventional generators are displaced by RESs, the inertial response also decreases. This leads to an increased rate-of-change-of-frequency (ROCOF), and a low frequency nadir (minimum frequency point) in a very short time. The primary frequency control cannot respond within the small time frame (typically less than 10 s) to arrest the system frequency change. This period is highlighted as section AB in Figure 3. It is clear from the figure that in systems with lower inertia, the frequency nadir is considerably lower along with a high ROCOF. Such situations can lead to tripping of frequency relays (causing under-frequency load shedding (UFLS)) and, in the worst case, may lead to cascaded outages [12,13]. The solution to such scenarios is to add virtual inertia in the system. The basic requirements of a virtual inertia system is that it has to operate in a very short time interval (typically less than 10 s) and in autonomous fashion. Deployed appropriately, virtual inertia systems would enhance system stability and enable greater penetration of RESs.

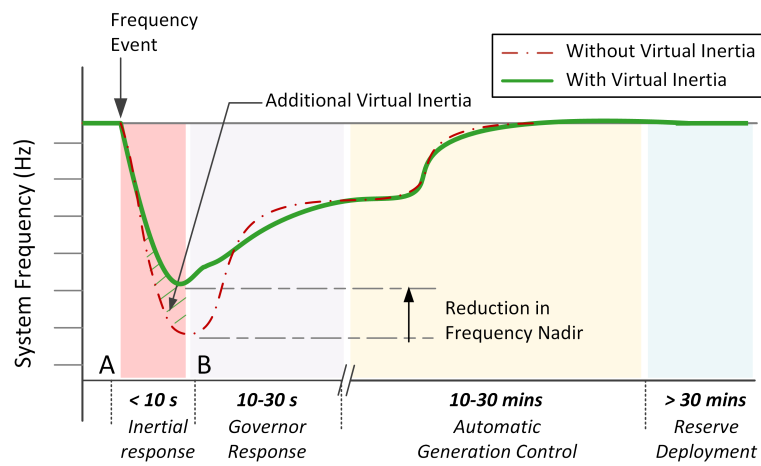


**Figure 3.** Multiple time-frame frequency response in a power system following a frequency event.

This paper presents a literature review of the various topologies used for virtual inertia implementation. The major topologies and the consequent improvements in these topologies are reviewed through a literature search followed by a restudy through simulations. The problem of large frequency variations due to high penetration of RESs are introduced first in Section 2. The “first generation” of virtual inertia systems are introduced next in Section 3. The topologies and control algorithms to effectively emulate inertia of synchronous generators (SGs) through power electronic based converters are discussed. After a literature review of the virtual inertia topologies, three main topologies are compared and evaluated in a common benchmark in Section 4. The “second generation” of virtual inertia systems is then reviewed in Section 5. The optimization of these systems in terms of dynamic performance and energy usage is discussed. Finally, a review of the challenges involved with integrating virtual inertia systems into the existing power system and some future research directions are discussed in Section 6. Section 7 discusses the conclusions of the paper.

## 2. Frequency Variations in Weak Power Systems with High Penetration of RES

Microgrids have been identified as the best option to integrate distributed generation (DG) units in terms of flexibility and reliability [14–16]. The microgrids can be operated in three possible modes: grid-connected, islanded, or isolated. A microgrid is said to have been islanded when a microgrid that is grid-connected disconnects from the grid, either in a planned fashion or due to a fault/disturbance in the main grid. In the isolated mode of operation, the microgrid is designed such that it is never connected to the grid. Regardless, these microgrid systems represent weak power systems and the high penetration of inertia-less PV and wind energy systems has a severe effect on the frequency stability. The rapid changes in the generation can cause frequency variations in the system that are outside standard limits and compromise the stability of the system.

Figure 4 shows the recommended standard frequency range for grid-connected and isolated/islanded microgrids. In the grid-connected mode, the frequency is controlled by the main grid and the frequency deviations are relatively small. However, this scenario is slowly changing with increased integration of large-scale inertia-less generation. The Institute of Electrical and Electronic Engineers (IEEE) recommends a tight frequency operating standard of  $\pm 0.036$  Hz for grid-connected systems. The North American Reliability Corporation (NERC) recommends triggering the first level of UFLS when the system frequency drops below 59.3 Hz (for a nominal frequency of 60 Hz for the US power grid). The activation of UFLS is the last automated reliability measure to counteract frequency drop and re-balance the system [17]. NERC recommended control actions include disconnecting the generator if the frequency drops below 57 Hz or rises above 61.8 Hz [18]. The European Norm EN50160 also imposes similar tight ranges for grid-connected microgrid systems [19]. There are no specific standards defined for frequency limits for isolated microgrid systems. This is highly dependent on the generation and the load mix in a particular microgrid system. From a generator point-of-view, frequency standards like the ISO 8528-5 standard [20] can provide a guideline for the frequency limits. With the small amount of SGs in isolated microgrids, the frequency excursions and ROCOF are greater and the need for virtual inertia is of high importance. In such isolated microgrids, to implement virtual inertia, either dedicated energy storage systems (ESSs) can be used [21,22], or inertia can be emulated by operating PV/wind below their maximum power point (MPP) [23,24]. However, the allowable frequency nadirs and ROCOFs in the microgrids in islanded/isolated conditions may be relaxed compared to grid-connected operation. This will be especially vital for the design of virtual inertia systems for isolated microgrids as these microgrids often have limited energy resources and relaxing the frequency operating region would result in significant energy saving and reduction in power ratings of virtual inertia systems.

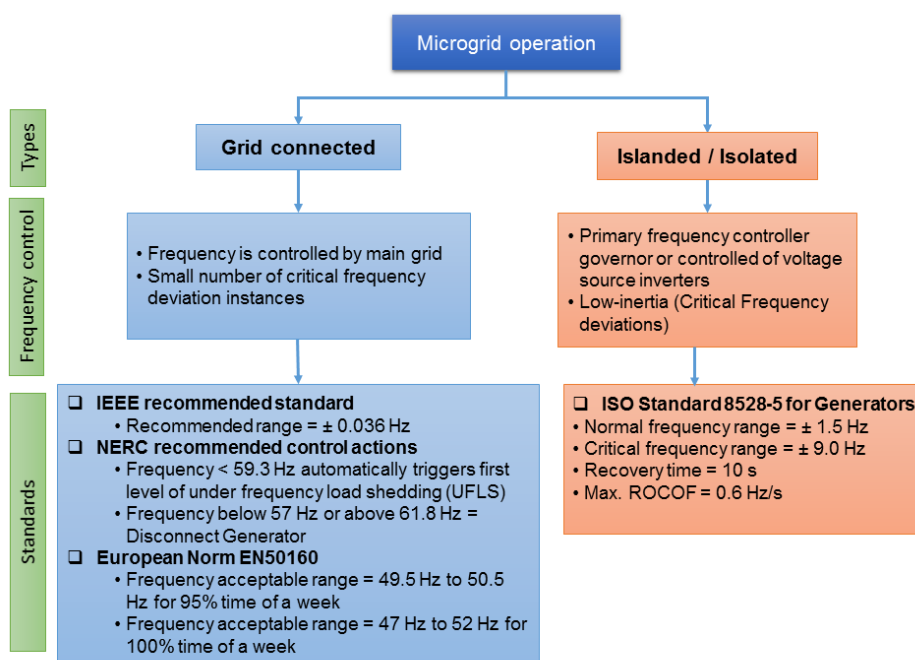


Figure 4. Frequency standards for microgrid systems [18–20].

### 3. First Generation: Virtual Inertia Topologies

#### 3.1. Concept and Classification of Virtual Inertia Topologies

The frequency variation in a power system after a frequency event/disturbance can be approximated by the swing equation [25]:

$$P_{gen} - P_{load} = \frac{d(E_{K.E.})}{dt} = \frac{d(\frac{1}{2}J\omega_g^2)}{dt} \quad (1)$$

$$P_{gen} - P_{load} = J\omega_g \frac{d\omega_g}{dt} \quad (2)$$

where,  $P_{gen}$  is the generated power,  $P_{load}$  is the power demand including losses,  $J$  is the total system inertia, and  $\omega_g$  is the system frequency. The inertia constant of the power system  $H$  is the kinetic energy normalized to apparent power  $S_g$  of the connected generators in the system:

$$H = \frac{J\omega_g^2}{2S_g} \quad (3)$$

Equation (2) can then be written as:

$$\frac{2H}{\omega_g} \frac{d\omega_g}{dt} = \frac{P_{gen} - P_{load}}{S_g} \quad (4)$$

Equation (4) can also be represented in terms of frequency (Hz) instead of angular frequency (rad/s) as follows:

$$\frac{2H}{f} \frac{df}{dt} = \frac{P_{gen} - P_{load}}{S_g} \quad (5)$$

where,  $\frac{df}{dt}$  is the ROCOF of the system. With reduced inertia, the ROCOF of the system increases which causes larger changes in frequency of the system in the same time-frame. Thus, the system requires additional inertia as more RESs are integrated into the power system. The concept of virtual inertia implementation using power electronic converters was first developed by Beck and Hesse [26]. Many other topologies and approaches have been developed in the literature since.

Virtual inertia is a combination of control algorithms, RESs, ESSs, and power electronics that emulates the inertia of a conventional power system [13]. The concept of virtual inertia is summarized in Figure 5. The core of the system is the virtual inertia algorithm that presents the various energy sources interfaced to the grid through power electronics converters as SGs. Most modern wind turbines are operated as variable speed wind turbines and interfaced through back-to-back converters, completely decoupling the inertia from the grid. Similarly, PV systems and ESSs have a DC-DC converter and an inverter in the front-end, and do not contribute to the inertial response [4,27]. Virtual inertia systems based on current/voltage feedback from the inverter output generate appropriate gating signals to present these resources as SGs from the point-of-view of the grid [28]. Although the basic underlying concepts are similar among the various topologies in the literature, the implementation is quite varied based on the application and desired level of model sophistication. Some topologies try to mimic the exact behavior of the SGs through a detailed mathematical model that represent their dynamics. Other approaches try to simplify this by using just the swing equation to approximate the behavior of SGs, while others employ an approach which makes the DG units responsive to frequency changes in the power system. This section discusses the various topologies that have been proposed in literature. Figure 6 shows a general classification of various topologies that are available in the literature for virtual inertia implementation. Among the listed topologies, the synchronverter, the Ise lab's topology, the virtual synchronous generator (most popular in literature from each classification), and the droop

control were selected for a detailed description. A brief description of the remaining topologies is also presented under Section 3.6.

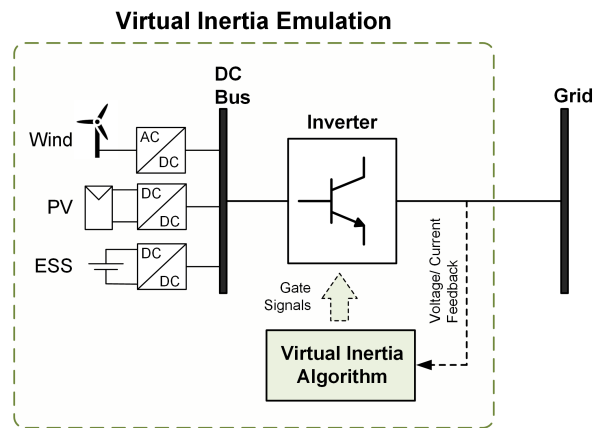


Figure 5. Concept of virtual inertia.

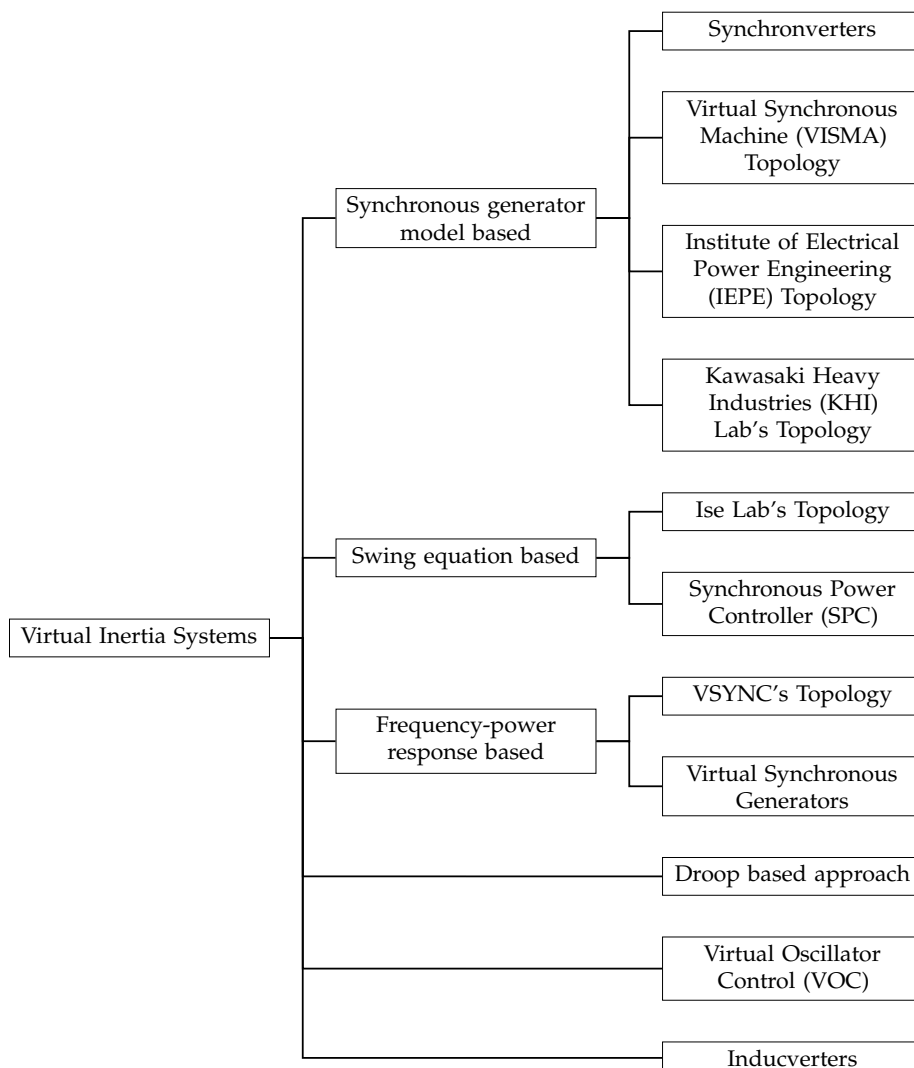


Figure 6. Classification of different topologies used for virtual inertia implementation.

### 3.2. Synchronverters: A Synchronous Generator Model Based Topology

Synchronverters operate the inverter-based DG units as SGs representing the same dynamics from the point-of-view of the grid [29]. This is based on the notion that such a strategy allows traditional operation of the power system to be continued without major changes in the operation structure. The topology is well developed in the literature by Q.C. Zhong [30]. A frequency drooping mechanism is used to regulate the power output from the inverter similar to how the SG regulates its power output [31]. The following basic equations are used to capture the dynamics of the SG:

$$T_e = M_f i_f \langle i, \widetilde{\sin\theta} \rangle \tag{6}$$

$$e = \dot{\theta} M_f i_f \widetilde{\sin\theta} \tag{7}$$

$$Q = -\dot{\theta} M_f i_f \langle i, \widetilde{\cos\theta} \rangle \tag{8}$$

where,  $T_e$  is the electromagnetic torque of the synchronverter,  $M_f$  is the magnitude of the mutual inductance between the field coil and the stator coil,  $i_f$  is the field excitation current,  $\theta$  is the angle between the rotor axis and one of the phases of the stator winding,  $e$  is the no load voltage generated, and  $Q$  is the generated reactive power. In Equations (6) and (8),  $\langle \cdot, \cdot \rangle$  represents the standard inner product of two vectors in  $\mathbb{R}^3$ . The three-phase stator current,  $i$ ,  $\widetilde{\sin\theta}$ , and  $\widetilde{\cos\theta}$  are vectors defined as follows:

$$i = \begin{bmatrix} i_a \\ i_b \\ i_c \end{bmatrix}; \widetilde{\sin\theta} = \begin{bmatrix} \sin\theta \\ \sin(\theta - \frac{2\pi}{3}) \\ \sin(\theta - \frac{4\pi}{3}) \end{bmatrix}; \widetilde{\cos\theta} = \begin{bmatrix} \cos\theta \\ \cos(\theta - \frac{2\pi}{3}) \\ \cos(\theta - \frac{4\pi}{3}) \end{bmatrix} \tag{9}$$

Equations (6)–(8) are first discretized and then solved in each control cycle in a digital controller to generate the gating signals for the DG unit under consideration. Figure 7a shows the basic schematic of the synchronverter. The dashed box represents the control part of the synchronverter, the details of which are illustrated in Figure 7b. The inverter output current  $i$  and grid voltage  $v$  are the feedback signals utilized to solve the differential equations within the controller. Additionally, the desired moment of inertia  $J$  and damping factor  $D_p$  can be set as desired. The selection of these parameters is crucial from the point-of-view of the stability of the system as shown in [32]. The frequency and voltage loops, as indicated in Figure 7b, are used to generate the control inputs—the mechanical torque,  $T_m$  and  $M_f i_f$ . In the frequency loop,  $T_m$  is generated from the reference active power  $P^*$  based on the nominal angular frequency of the grid  $\omega_n$ . The virtual angular frequency of the synchronverter  $\omega$  is thus generated by this loop which is integrated to calculate the phase command  $\theta$  and is used for the pulse width modulation (PWM). Similarly, in the voltage loop, the difference between the reference voltage  $v^*$  and the amplitude of the grid voltage  $v$  is multiplied by a voltage drooping constant  $D_q$ . This is added to the error between the reference reactive power  $Q^*$  and the reactive power  $Q$  calculated using (8). The resulting signal is then passed through an integrator with gain  $\frac{1}{k_v}$  to generate  $M_f i_f$ . The outputs of the controller are  $e$  and  $\theta$  which are used for PWM generation.

The underlying equations of a synchronverter topology form an enhanced phase locked loop (PLL) or a sinusoid-locked loop, making it inherently capable of maintaining synchronism with the terminal voltage [33]. Single phase variants of the synchronverter have also been designed in [34]. The basic version of synchronverter requires a PLL to initially synchronize with the grid, however the use of PLLs in weak grids is known to be prone to instabilities [35–37]. To counteract this, self-synchronized synchronverters are introduced in [38]. The synchronverter topology has also inspired the operations of rectifiers as synchronous motors [39] which helps in obtaining inertial response from the load side of the power system. Moreover, the voltage-source based implementation means that synchronverters can be operated as grid forming units, and ideally suited for inertia emulation from DGs that are not connected with the main grid. The fact that the frequency derivative is not required for the implementation, is a major advantage as derivative terms often induce noise in the system. Although the synchronverter is able to replicate the exact dynamics of a SG, the complexity of the differential

equations used can result in numerical instability. Moreover, a voltage-source based implementation means there is no inherent protection against severe grid transients, which may result in need of external protection systems for safe operation.

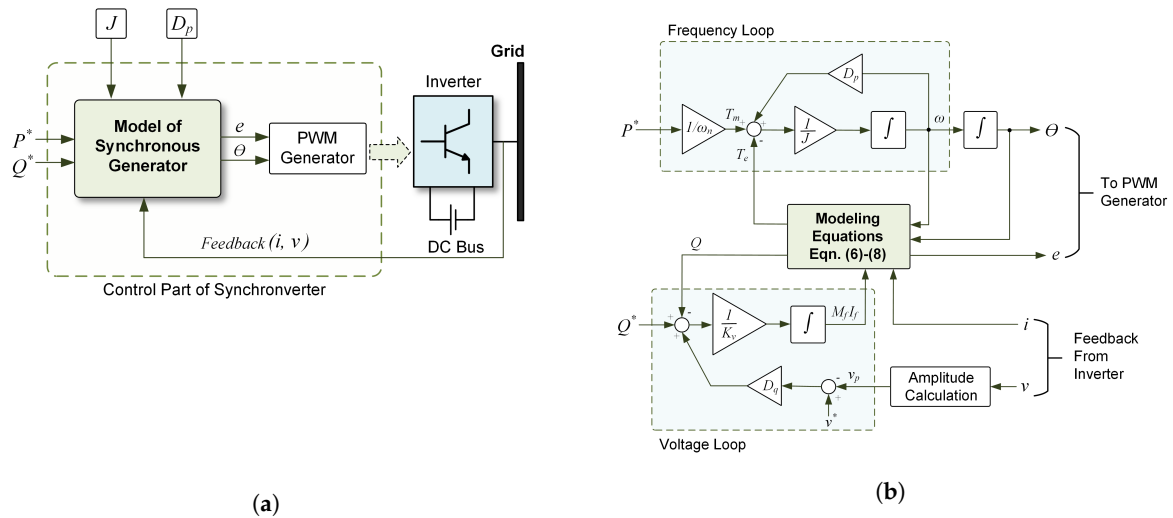


**Figure 7.** Synchronverter topology: (a) overall schematic showing operating principle; (b) detailed control diagram showing the modeling equations.

### 3.3. Ise Lab's Topology: A Swing Equation Based Topology

The topology developed by Ise lab for virtual inertia implementation is similar to the synchronverter approach described previously, but instead of using a full detailed model of the SG, the topology solves the power-frequency swing equation every control cycle to emulate inertia [40]. The schematic diagram of the topology illustrating the operation principle is shown in Figure 8a. The controller senses the inverter output current  $i$  and the voltage of the point of connection  $v$ , and computes the grid frequency  $\omega_g$  and active power output of the inverter  $P_{out}$ . These two parameters are inputs to the main control algorithm block along with  $P_{in}$  which is the prime mover input power [41]. Within the control algorithm, the swing equation given by Equation (10) is solved every control cycle thus generating the phase command  $\theta$  for the PWM generator. The typical swing equation of a SG is:

$$P_{in} - P_{out} = J\omega_m \left( \frac{d\omega_m}{dt} \right) + D_p \Delta\omega \tag{10}$$

$$\Delta\omega = \omega_m - \omega_g \tag{11}$$

where,  $P_{in}$ ,  $P_{out}$ ,  $\omega_m$ ,  $\omega_g$ ,  $J$ , and  $D_p$  are the input power (similar to the prime mover input power in a SG), the output power of the inverter, virtual angular frequency, grid/reference angular frequency, moment of inertia, and the damping factor, respectively. A model of the governor, as shown in Figure 8b, is utilized to compute the input power  $P_{in}$  based on the frequency deviation from a reference frequency  $\omega^*$ . The governor is modeled as a first-order lag element with gain  $K$  and time-constant  $T_d$ .  $P_0$  represents continuous power reference for the DG unit. The delay in the governor model leads to higher ROCOF and thus higher frequency nadirs as a consequence. The voltage reference  $e$  can be generated through  $Q - v$  droop approach as described in [42,43].

Similar to the synchronverter, derivative of frequency is not needed to implement the control algorithm. This is highly beneficial as frequency derivatives are known to introduce noise in the system which makes the system difficult to control. Additionally, this topology can be used to operate DG units as grid forming units. However, problems related to numerical instability still remain, which along with improper tuning of parameters  $J$  and  $D_p$ , can lead to oscillatory system behavior [41].

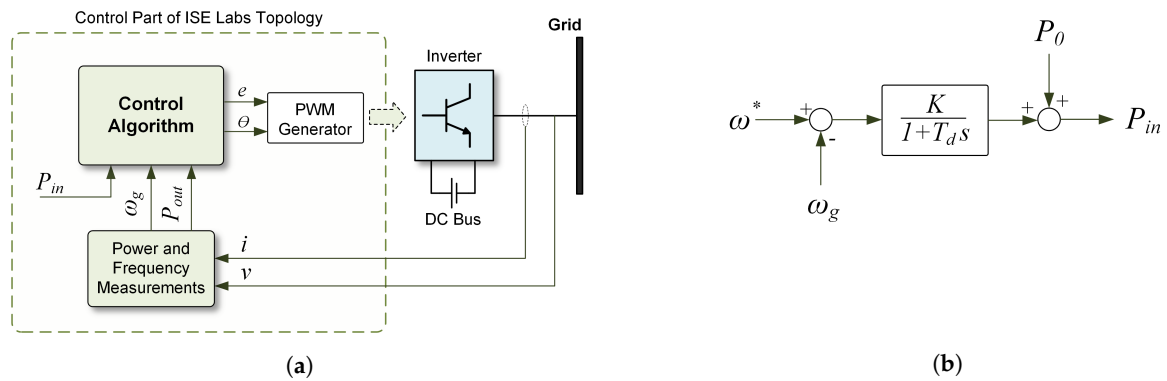


**Figure 8.** Ise Lab’s topology: (a) overall schematic showing operating principle; (b) the governor model to compute input power.

### 3.4. Virtual Synchronous Generators: A Frequency-Power Response Based Topology

The main idea behind virtual synchronous generators (VSG) is to emulate the inertial response characteristics of a SG in a DG system, specifically the ability to respond to frequency changes [25,44]. This emulates the release/absorption of kinetic energy similar to that of a SG, thus presenting the DG units as a dispatchable source [45,46]. Compared to traditional droop controllers which provide only frequency regulation, the VSG approach is able to provide dynamic frequency control [21]. This dynamic control is based on the derivative of the frequency measurement and behaves similarly to inertial power release/absorption by a SG during a power imbalance. Thus, the VSG is a dispatchable current source that regulates its output based on system frequency changes. This is one of the simplest approaches to implement virtual inertia in DG systems as it does not incorporate all the detailed equations involved in a SG. However, operating multiple DG units as current sources is known to result in instability [47].

The output power of the VSG converter is controlled using Equation (12):

$$P_{VSG} = K_D \Delta\omega + K_I \frac{d\Delta\omega}{dt} \quad (12)$$

where,  $\Delta\omega$  and  $\frac{d\Delta\omega}{dt}$  represent the change in angular frequency and the corresponding rate-of-change.  $K_D$  and  $K_I$  represent the damping and the inertial constant, respectively. The damping constant is similar to the frequency droop and helps return the frequency to a steady-state value and reduce the frequency nadir. The inertial constant arrests the ROCOF by providing fast dynamic frequency response based on the frequency derivative. This feature is especially important in an isolated grid where the initial ROCOF can be very high, leading to unnecessary triggering of protection relays. The VSG topology is illustrated in Figure 9. A PLL is used to measure the change in system frequency and ROCOF [45]. Then, using Equation (12), the active power reference for the inverter is computed. The current references are then generated for the current controller based on this reference power. The topology illustrated here assumes a direct-quadrature ( $d-q$ ) based current control approach, but any other current control techniques (as described in [48,49]) may be used. For  $d-q$  control,  $d$ -axis current reference can be calculated as [22]:

$$I_d^* = \frac{2}{3} \left( \frac{V_d P_{VSG} - V_q Q}{V_d^2 + V_q^2} \right) \quad (13)$$

where,  $V_d$  and  $V_q$  are the  $d$  – axis and  $q$  – axis components of the measured grid voltage  $v$ . The  $q$ -axis current reference  $I_q^*$  and the reactive power  $Q$  is set to zero as it is assumed that only the active power is being controlled. The current controller based on the grid current feedback generates the gate signals to drive the inverter. Thus, the inverter behaves as a current-controlled voltage source inverter [13,48].

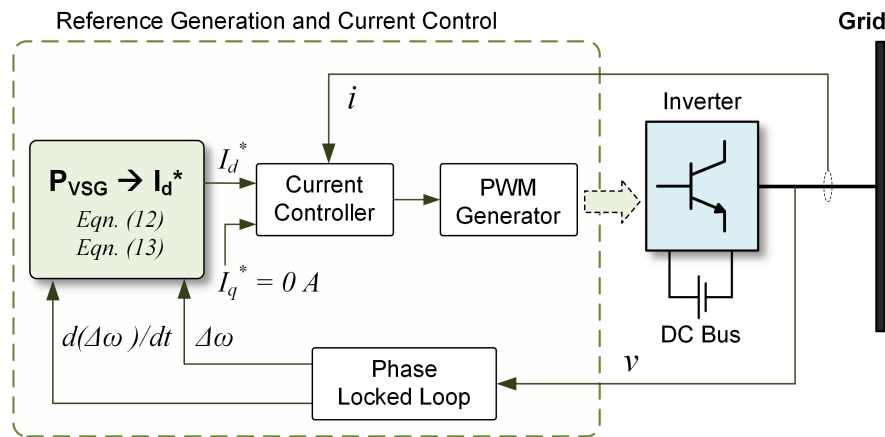


Figure 9. Virtual synchronous generator (VSG) topology.

This topology is used by the European VSYNC research group [45,50] and has demonstrated the effectiveness of inertia emulation using VSG topology through real-time simulations [51] and several field tests [52]. In [22], an experimental verification of the topology is presented for remote microgrid applications. The VSG topology has also been widely employed for virtual inertia emulation from wind systems as reported in [6,53,54]. The main drawback of this topology is that it cannot be implemented in islanded modes where the virtual inertia unit has to operate as a grid forming unit. Moreover, the system emulates inertia during frequency variations, but not in input power variations [55]. Accurate measurement of the frequency derivative through PLLs can be challenging for this kind of implementation [56,57]. The performance of PLLs can degrade and compete against each other, especially in weak grids [58,59]. PLL systems are known to show steady-state errors and instability especially in weak grids with frequency variations, harmonic distortions, and voltage sags/swells [35–37]. In [60], it was shown that the problems with instability are even more pronounced when a proportional-integral (PI) controller is used to implement the inner-current control loop of the inverter. Accordingly, a VSG requires a robust and sophisticated PLL for a successful implementation [61]. Another disadvantage of the VSG approach is that the derivative term used to compute the ROCOF makes the VSG sensitive to noise which can lead to unstable operation.

### 3.5. Droop-Based Approaches

The approaches described so far try to mimic or approximate the behavior of SGs to improve inertial response of inverter-dominated power systems. Different from these techniques, the frequency-droop based controllers have been developed for autonomous operation of isolated microgrid systems [62,63]. Based on the assumption that the impedance of the grid is inductive, the frequency droop is implemented as:

$$\omega_g = \omega^* - m_p(P_{out} - P_{in}) \tag{14}$$

where,  $\omega^*$  is the reference frequency,  $\omega_g$  is the local grid frequency,  $P_{in}$  is the reference set active power,  $P_{out}$  is the measured active power output from the DG unit, and  $m_p$  is the active power droop. Similarly, the voltage-droop is implemented as:

$$v_g = v^* - m_q(Q_{out} - Q_{in}) \tag{15}$$

where,  $v^*$  is the reference voltage,  $v_g$  is the local grid voltage,  $Q_{in}$  is the reference set reactive power,  $Q_{out}$  is the measured reactive power output from the DG unit, and  $m_q$  is the reactive power droop.

The schematic of a frequency-droop controller based on Equation (14) is shown in Figure 10. Often a low pass filter with a time constant  $T_f$  is used when measuring the output power to filter out high frequency components from the inverter [14]. In the literature [59,64,65], it has already been shown that the use of this filter makes the droop-based control approximate the behavior of virtual inertia systems. The proof was first presented by Arco et al. [59] and is repeated here for convenience.

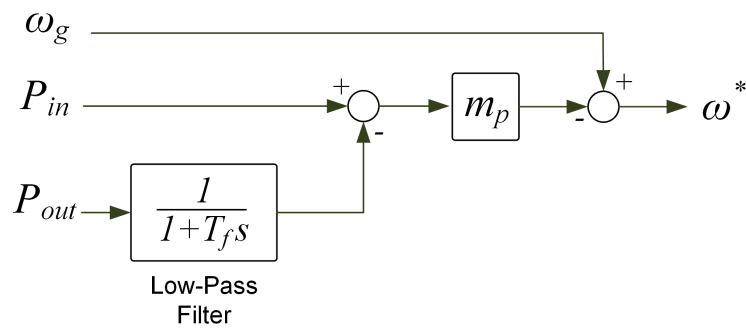


Figure 10. Schematic for frequency droop control.

**Proof.** Based on the schematic of Figure 10:

$$P_{out} = (1 + T_f s) \left\{ \frac{1}{m_p} (\omega_g - \omega^*) + P_{in} \right\} \tag{16}$$

Rearranging,

$$P_{in} - P_{out} = \frac{1}{m_p} (\omega^* - \omega_g) + T_f \cdot \frac{1}{m_p} \cdot s \cdot \omega^* \tag{17}$$

□

This equation is of the similar form of the virtual synchronous generator described in Equation (12). The exact approximation is as follows:

$$K_I = T_f \cdot \frac{1}{m_p} \tag{18}$$

$$K_D = \frac{1}{m_p} \tag{19}$$

Hence, the filters used for power measurements in these controllers constitute a delay which is mathematically equivalent to virtual inertia, while the droop gain is equivalent to damping. However, the traditional droop-based systems described by Equations (14) and (15) are known to have slow transient response. Moreover, the inductive grid assumption may not always be valid. Methods to improve the droop controllers, such as using virtual output impedance [16] or improving dynamic behavior of the droop scheme [14], have been proposed. In [10,66], a technique to emulate virtual inertia by a modified droop approach was also presented.

### 3.6. Other Topologies

Some other topologies that have been proposed in the literature are—virtual synchronous machine, referred to as “VISMA” in the literature, Institute of Electrical Power Engineering (IEPE’s) topology, Kawasaki Heavy Industries (KHI) lab’s topology, synchronous power controllers (SPC), virtual oscillators, inducverters, etc. The basic concept of inertia emulation remains the same in all these techniques. The VISMA topology as proposed in [67] uses  $d$ - $q$  (synchronous reference frame) based

mathematical model of a SG. This model when implemented in the digital controller of a power inverter replicates the dynamics of a SG. Instantaneous measurements of the grid voltage are used to compute the stator currents of the virtual machine and these currents are injected through a hysteresis current control approach using a power inverter. However, concerns with numerical instability have been reported with the VISMA model [68]. To improve robustness, a three-phase model has been proposed in [69] over a  $d$ - $q$  based model. This is especially effective under unsymmetrical load conditions or rapid disturbances in the grid. A comparison between the VISMA algorithm implemented as a current source versus a voltage source has also been performed in [70]. The VISMA model implemented as a voltage source is referred to as IEPE's topology in the literature [28]. Instead of using voltage as input as with the VISMA topology, IEPE's topology uses the DG output current as input and generates reference voltages for the virtual machine. The IEPE topology is better suited for islanded operation, but transient currents particularly during the synchronization processes when operated in grid-connected mode can be difficult to deal with. In the KHI topology, instead of using detailed dynamic model of SG, an equivalent governor and automatic voltage regulator (AVR) model is implemented in a digital controller to generate voltage amplitude and phase reference for the virtual machine [71]. The reference is then used to generate current references based on algebraic-phasor representation of the SGs.

Another popular topology for virtual inertia implementation is the SPC as proposed in [72–74]. The general structure of the control algorithm is similar to the structure proposed in the Ise lab's topology, but instead of operating the converter as a voltage controlled system or a current controlled system, it implements a cascaded control system, with an outer voltage loop and an inner current control loop through the use of a virtual admittance. In general, such a cascaded control structure provides inherent over-current protection during severe transient operating conditions. This is lacking in other open-loop approaches such as synchronverters or the Ise lab's topology [75] described previously. SPC also avoids the discontinuities encountered in solving the mathematical models, thus making the system more robust against numerical instabilities. The nested loop structure however does entail complexity in tuning the control system parameters. Furthermore, at its core, instead of using the swing equation for inertia emulation, a second order model with an over-damped response is proposed. This helps to reduce the oscillations in the system [55]. Improved forms of this second-order model was presented in [55,76].

Inducverters [58] are one of the recent topologies that has been proposed which tries to mimic the behavior of induction generators instead of SGs. This method has the advantage of auto-synchronization without a PLL [77]. A virtual-inertia based static synchronous compensator (STATCOM) controller was proposed in [65] which behaves as synchronous condenser. The virtual inertia controller was used to exploit the fact that no PLL is required, hence providing improved voltage regulation compared to traditional STATCOMs with PLL units. Virtual oscillator controller (VOC) is another approach where, instead of mimicking synchronous/induction generators, a non-linear oscillator is implemented within the controller to synchronize DG units without any form of communication [78,79]. This approach is particularly beneficial for a grid largely dominated with DGs, as the controller is intrinsically able to maintain synchronism and share the total system load [80].

### 3.7. Summary of Topologies

A summary table which highlights the key features and weakness of various virtual inertia control topologies is presented in Table 1.

**Table 1.** Summary of Virtual Inertia Control Topologies.

Control Technique	Key Features	Weaknesses
Synchronous generator (SG) model based	<ul style="list-style-type: none"> <li>• Accurate replication of SG dynamics</li> <li>• Frequency derivative not required</li> <li>• Phase locked loop (PLL) used only for synchronization</li> </ul>	<ul style="list-style-type: none"> <li>• Numerical instability concerns</li> <li>• Typically voltage-source implementation; no over-current protection</li> </ul>
Swing equation based	<ul style="list-style-type: none"> <li>• Simpler model compared to SG based model</li> <li>• Frequency derivative not required</li> <li>• PLL used only for synchronization</li> </ul>	<ul style="list-style-type: none"> <li>• Power and frequency oscillations</li> <li>• Typically voltage-source implementation; no over-current protection</li> </ul>
Frequency-power response based	<ul style="list-style-type: none"> <li>• Straightforward implementation</li> <li>• Typically current-source implementation; inherent over-current protection</li> </ul>	<ul style="list-style-type: none"> <li>• Instability due to PLL, particularly in weak grids</li> <li>• Frequency derivative required, system susceptible to noise</li> </ul>
Droop-based approach	<ul style="list-style-type: none"> <li>• Communication-less</li> <li>• Concepts similar to traditional droop control in SGs</li> </ul>	<ul style="list-style-type: none"> <li>• Slow transient response</li> <li>• Improper transient active power sharing</li> </ul>

#### 4. Design Procedures and Simulation Results

In this section, three of the major virtual inertia topologies were restudied in a diesel generator based remote microgrid system. The design procedures and simulation results presented are aimed to supplement the concepts of virtual inertia topologies reviewed in Section 3. Three of the topologies—the synchronverter, the Ise lab’s topology, and the VSG—were implemented and their performance was studied in a common benchmark. Moreover, a procedure is provided to choose appropriate parameters for the virtual inertia systems. The three virtual inertia systems were designed in a common framework so that the different parameters used are more relatable to each other. To this end, constants in each topology were selected such that the virtual inertia system injects/absorbs the same amount of active power for a given frequency change. Furthermore, the inertial constant and the damping constant have the same proportion and were related through a time constant  $T_f$  of 0.01 s in all the simulations. This led to an inertia constant  $H$  of 1 s in all simulation cases for the virtual inertia unit. The schematic used for the virtual inertia simulation benchmark is shown in Figure 11. The generator was rated at 13 kVA, while the PV unit was rated at 6 kWp [22]. A separate, dedicated inverter unit rated at 10 kW was used as the virtual inertia unit. In all the cases, the steady-state power output from the inverter was set to 1000 W. It was assumed that, the DC side of the inverter was connected to a 400 V DC source which remained constant in all the simulations. Step changes in the load were used to emulate the change in load or PV generation in all the systems. For simplicity, the inverter was modeled as either a controlled current source or a controlled voltage source (depending on the virtual inertia topology used) neglecting the switching behavior.

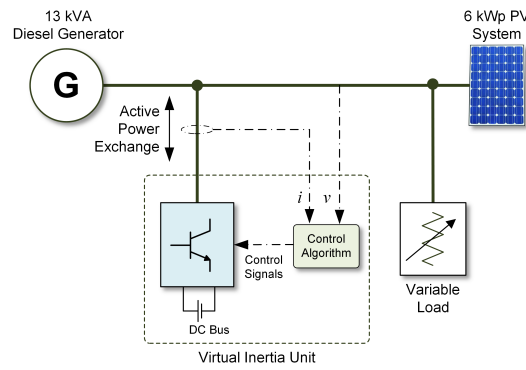


Figure 11. Schematic diagram of the virtual inertia simulation benchmark.

#### 4.1. Design of Synchronverter Topology

The main parameters to be computed to implement a synchronverter are the moment of inertia  $J$  and the damping factor  $D_p$ . The parameter  $D_p$  can be calculated using Equation (20) from [29].

$$D_p = -\frac{\Delta T}{\Delta \omega} = -\frac{\Delta P}{\omega_g \Delta \omega} \quad (20)$$

Once  $D_p$  was calculated, the moment inertia  $J$  was computed using the desired time constant for the system,  $\tau_f$ :

$$\tau_f = \frac{J}{D_p} \quad (21)$$

In this case,  $D_p$  was calculated to be 14.072 assuming  $\Delta P$  of 100% (10 kW) for 0.5% change in the angular frequency (1.885 rad/s). Then for a time-constant of 0.01 s, the  $J$  value was calculated to be 0.140. The inertia constant from the synchronverter is:

$$H = \frac{J \omega_g^2}{2P_{rated}} = 1 \text{ s} \quad (22)$$

The frequency and ROCOF of the system after a step-increase of 2 kW on the load, with and without the synchronverter, are presented in Figure 12a,b, respectively. The dip in frequency and the ROCOF of the system was reduced with the addition of the synchronverter, as expected. The additional inertia from the synchronverter increased the settling time for the frequency compared to when there was no synchronverter in the system. As shown in Figure 12c, the synchronverter increases its active power output in response to the frequency event much like the behavior of a SG.

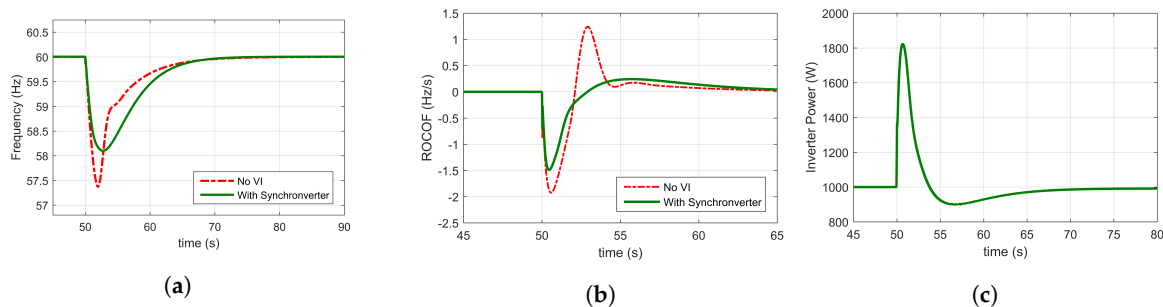
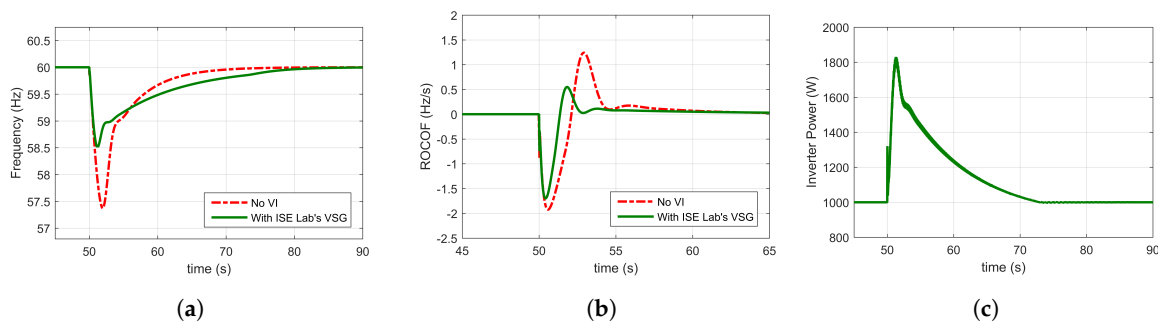


Figure 12. Simulation results from a synchronverter: (a) system frequency after a step-increase of 2 kW load; (b) ROCOF after a step-increase of 2 kW load; (c) increase in inverter power in response to system frequency decrease [29].

#### 4.2. Design of Ise Lab's Topology

For the design of the Ise lab's topology, the same values for the constants  $J$  and  $D_p$  that were calculated for synchronverter in Section 4.1 were used. For the implementation of the governor model, a  $K$  value of 0.01 with a time delay  $T_d$  of 0.16 s was used. The frequency and ROCOF of the system after a step-increase of 2 kW on the load, with and without the Ise lab's system, is presented in Figure 13a,b, respectively. The dip in the frequency and the ROCOF of the system was reduced with addition of the virtual inertia unit, as expected. The additional inertia from virtual inertia system increased frequency settling time compared to the case without the virtual inertia system. The settling time, however was higher than with the synchronverter. Figure 13c shows the power injected by the inverter during the step-load increase. There is a short transient at 50 s, which was a consequence of numerical oscillation in solving the swing equation. The peak-power injected was similar to that of the synchronverter, but the time taken for the power to return to the steady-state value of 1000 W was much longer, leading to a larger energy usage from the DC side.



**Figure 13.** Simulation results from ISE lab's topology: (a) system frequency after a step-increase of 2 kW load; (b) ROCOF after a step-increase of 2 kW load; (c) increase in inverter power as a response to system frequency decrease [40].

#### 4.3. Design of Virtual Synchronous Generator Topology

For implementing the VSG topology, the main parameters to be designed are the inertia constant  $K_I$  and the damping constant  $K_D$ . The parameter  $K_D$  can be calculated using:

$$K_D = \frac{\Delta P}{\omega_g \Delta \omega} \tag{23}$$

Once  $K_D$  was calculated, the inertia constant  $K_I$  was computed using the desired time constant for the system,  $\tau_f$ :

$$\tau_f = \frac{K_I}{K_D} \tag{24}$$

In this case, the damping constant,  $K_D$ , was calculated to be 14.07, assuming  $\Delta P$  of 100% (10 kW) for 0.5% change in the angular frequency (1.885 rad/s). Then, for a time-constant of 0.01 s, the  $K_I$  value was calculated to be 0.14. The inertia constant from the VSG is:

$$H = \frac{K_I \omega_g^2}{2P_{rated}} = 1s \tag{25}$$

The frequency and ROCOF of the system after a step-increase of 2 kW on the load, with and without the VSG, is presented in Figure 14a,b, respectively. The dip in frequency and the ROCOF of the system was reduced with addition of the VSG, as expected. As with the previous cases, the additional inertia from the VSG slowed the system down, and the settling time for the frequency was increased compared to the case without virtual inertia. The peak-power injected was slightly higher than that of the synchronverter and Ise lab's topology. However, the time taken for the power to return to the

steady value of 1000 W was much longer than for the synchronverter leading to a larger energy usage from the DC side.

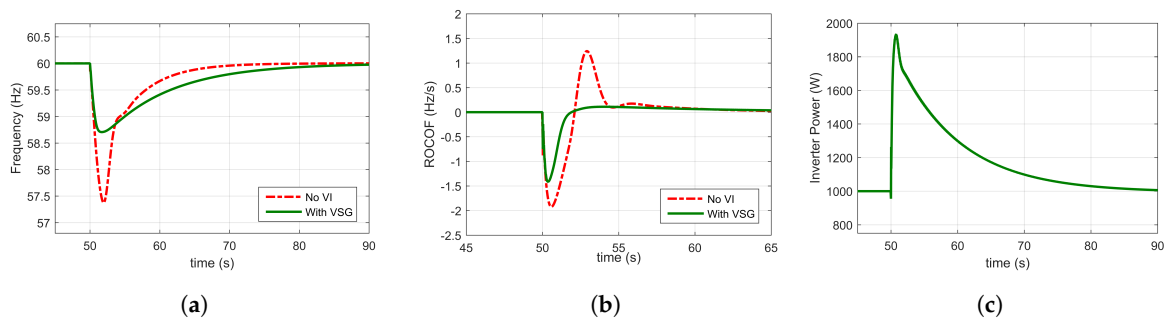


**Figure 14.** Simulation results from a virtual synchronous generator: (a) system frequency after a step-increase of 2 kW load; (b) ROCOF after a step-increase of 2 kW load; (c) increase in inverter power as a response to system frequency decrease [45,46].

#### 4.4. Summary of Simulations

The simulation results are summarized in Table 2 in terms of parameters like the minimum frequency, maximum ROCOF, settling time, peak power, and energy exchange. The settling time is defined here as the time required for the frequency to return to and stay within  $\pm 0.25$  Hz of the final steady-state frequency after a disturbance. The energy exchange was calculated over the time period where the inverter exchanges power with the system. With all three topologies, the minimum frequency and ROCOF were reduced by similar amounts. The peak power delivered by the inverter varied slightly, with the highest value of 1929 W for the VSG topology. The most pronounced differences were in the settling time for the frequency and the energy exchange. Compared to systems with no virtual inertia, the settling time has increased in all three cases. This was expected as adding virtual inertia slows down the frequency dynamics. The ISO8528-5 standard for generators sets recommends a settling time of 10 s [20]. The settling time, however, increased to 13.2 s with synchronverter and an even higher value of 17.7 s and 17.9 s with the Ise lab’s and VSG respectively. This led to a relatively higher energy exchange in these two topologies of 3.8 Wh and 4.9 Wh compared to that 0.8 Wh with the synchronverter. Moreover, there was a short-energy recovery period in the power plot of the synchronverter as seen in Figure 12c which led to a lower energy exchange estimate for the synchronverter.

**Table 2.** Performance comparison of systems without virtual inertia (VI), and VI implemented through synchronverter, Ise lab’s and virtual synchronous generator (VSG) topologies.

Parameter	No VI	Synchronverter	Ise Lab	VSG
Minimum Frequency	57.3 Hz	58.1 Hz	58.6 Hz	58.3 Hz
Maximum ROCOF	1.9 Hz/s	1.5 Hz/s	1.6 Hz/s	1.7 Hz/s
Settling time	11.3 s	13.2 s	17.7 s	17.9 s
Peak power delivered	0 W	1825 W	1800 W	1929 W
Energy exchanged	0 Wh	0.8 Wh	3.8 Wh	4.9 Wh

Therefore, by appropriate selection of the parameters for the topologies through the time constant  $T_f$  and/or the inertia constant  $H$ , similar inertial response can be achieved in terms of frequency deviation reduction and power exchange from the inverter. Based on the topology, the exact dynamics represented by the system may vary. The selection of a particular topology depends on the application and the desired level of replication of the dynamics of the SG. Topologies like the synchronverter and the Ise lab’s topology may be more suitable for isolated power system as they can operate autonomously as grid forming units, as well as for reasons discussed in Section 3. The VSG topology on the other hand behaves more like a grid following unit with added inertial response capabilities

and is more suited towards interconnected operations. The synchronverter or Ise lab's topology are more suitable for a closer approximation of SG dynamics. If the main aim, however, is to make the DG unit responsive to frequency changes, the VSG approach provides a far simpler implementation.

## 5. Second Generation: Optimization of Virtual Inertia Systems

The first generation of virtual inertia systems in the literature focused on developing novel topologies for emulation of inertia using power electronic converters. These topologies have matured since as pointed out in Section 3. Recently, the field is more focused towards improving and optimizing the performance of these topologies from the point-of-view of enhanced dynamics, stability, and minimizing energy storage requirements.

### 5.1. Second Generation of Synchronverters

Improved versions of the synchronverter have been proposed in [81,82] which makes the synchronverter more robust and allows for an more accurate dynamic representation of SGs. One of the main improvements (among others) in [82] is virtually increasing the filter inductance of the synchronverter, which improved the stability compared to the original synchronverter. This modification allowed for an improved control over the response speed of the frequency loop proposed in [29]. In a similar theme, an auxiliary loop around the frequency-loop was proposed in [83] which allowed for a free control of the response speed of synchronverter. This auxiliary loop did not affect the steady-state drooping mechanism of the synchronverter which is very desirable. By changing the inertia constant  $J$  and a different tunable constant  $D_f$ , the desired response speed was achieved. In [84], a synchronverter with analytically determined bounds for frequency and voltage was introduced. In traditional synchronverters, saturation units were employed for this purpose, but such an approach can lead to instability due to wind-up. Instead, analytically determined bounds based on the system parameters were proposed to improve stability.

### 5.2. Second Generation of Ise Lab's Topology

In the traditional Ise lab's topology, active power oscillation during the inertia emulation has been identified as one of the major concerns [41]. Typically, during a frequency event, the DG unit needs to release/absorb a high amount of power, which may exceed their power ratings. This is not a problem for conventional SGs as they have inherently overrated operation capabilities. However, in the case of inverters, the switches have to be over-sized to handle such peak power, leading to an increase in inverter size and, consequently, cost [36]. In [41], an alternating moment of inertia emulation approach was proposed to make the system less susceptible to such oscillations. The  $J$  parameter was changed based on the relative "virtual angular velocity" and its rate of change. The proposed alternating moment of inertia approach not only stabilized the system under consideration, but other nearby virtual inertia units as well. Similarly, in [85] another technique of adjusting the "virtual stator reactance" of the virtual inertia unit has also been proposed to reduce such active power oscillations. This approach was somewhat similar to the approach described for synchronverters in [82]. The technique was also found to aid in proper transient active power sharing when operating multiple virtual inertia units in a microgrid environment. In [86], a particle swarm optimization technique was developed to properly tune the parameters of the system and achieve smooth transitions after a disturbance when operating multiple virtual inertia units.

### 5.3. Second Generation of Virtual Synchronous Generators

In terms of improvement in VSG topologies, some researchers have developed techniques to try to minimize the frequency nadirs/peaks in the system at the expense of higher energy usage and peak transient power exchange through the virtual inertia systems [87,88]. Other researchers, meanwhile, have focused on reducing the energy storage requirements and limiting peak transient power in virtual inertia systems even though it leads to slightly higher frequency nadirs/peaks [89,90]. A self-tuning

VSG was developed in [89] using an online optimization technique to tune the  $K_I$  and  $K_D$  parameters of the VSG control algorithm (described in Section 3.4) to minimize the frequency excursions, the ROCOF, and the power flow through the ESS. Although the frequency excursions were slightly higher in the case of the self-tuning algorithm, the power flow through the ESS was reduced by 58%. Moreover, the technique used less energy per Hz of frequency reduction than a constant parameter VSG.

On a similar note of energy saving, an online neural-network based controller was proposed in [90,91]. It used an adaptive dynamic programming (ADP) based approach to optimize the system and minimize energy usage while limiting the transient power. The controller supplemented the power references generated by the main VSG algorithm  $P_{VSG}$  with a supplementary signal  $P_{ADP}$  to give the total reference  $P_{VSG,TOTAL}$  as shown in Figure 15a. The aim of this supplementary signal was to improve the dynamics of virtual inertia. The proposed ADP controller used a neural network structure with two different networks—an action network and a critic network as shown in Figure 15b. The idea behind the design of the critic network was to adapt its weight such that the optimal cost function  $J^*(X(t))$  satisfies the Bellman principle of optimality as given by:

$$J^*(X(t)) = \min_{u(t)} \{J^*(X(t+1)) + r(X(t)) - U_c\} \tag{26}$$

where,  $r(t)$  is the reinforcement signal for the critic network and  $U_c$  is a heuristic term used to balance. The input to the supplementary ADP controller was the state vector  $X(t)$  where the elements were the frequency error and the one and two time-step delayed frequency error signals. Based on a reinforcement learning approach, the ADP controller generated auxiliary power reference signals  $P_{ADP}$  to return the frequency back to its steady-state value faster and as a consequence reduced the energy exchange as explained in [90,91]. The main concern with adding virtual inertia to the system is that it can increase the frequency settling time, leading to increased energy exchange from the ESS, which subsequently shortens the life of the ESS. The online controller was able to reduce the frequency settling time and the transient peak power. Figure 16a shows the frequency of a PV-hydro system under step load changes with and without the ADP controller. The frequency excursion was slightly higher than using constant parameter VSG, but there was a reduction in the frequency settling time. This led to lower energy usage and lower transient power as observable in Figure 16b. Table 3 summarizes the improvement achieved through the ADP-based virtual inertia controller.

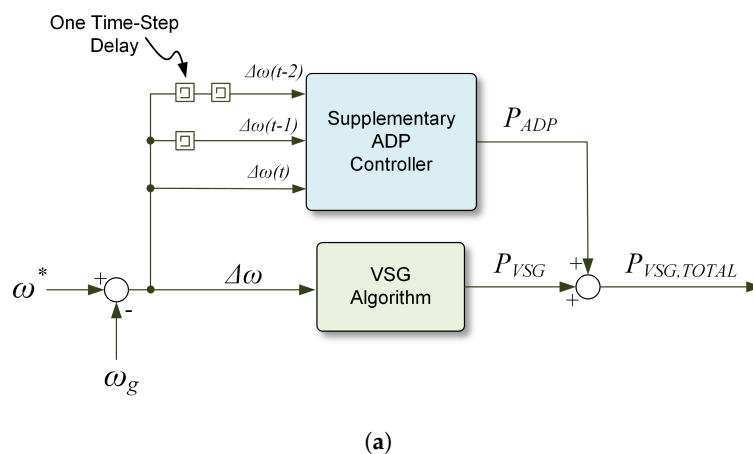
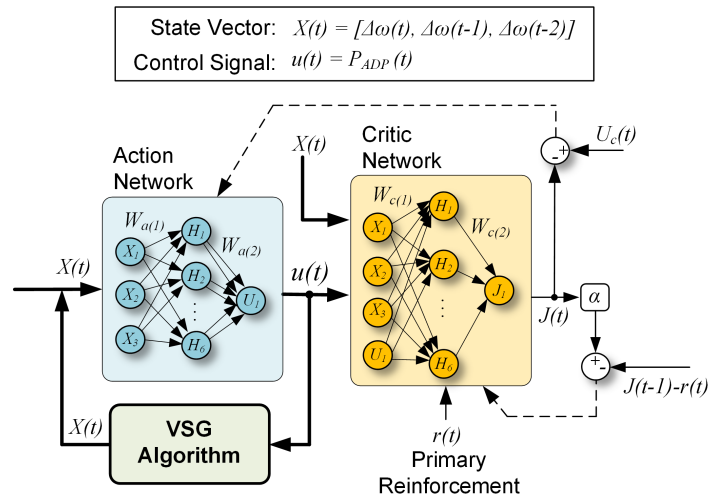
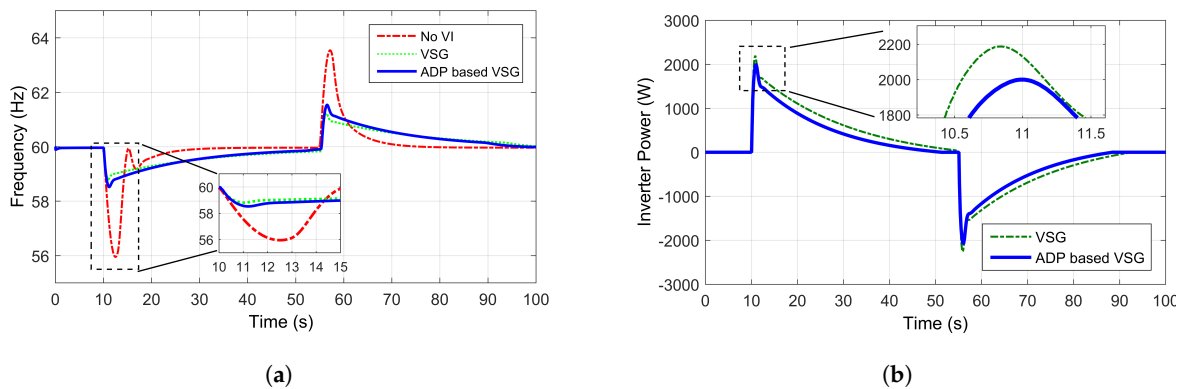


Figure 15. Cont.



(b)

**Figure 15.** Modified virtual synchronous generator (VSG) using adaptive dynamic programming (ADP) (a) overall schematic of the controller; (b) the action and critic neural network based structure.



(a)

(b)

**Figure 16.** Comparison of traditional virtual synchronous generator (VSG) controller with the online learning based controller: (a) frequency of the system for step load changes; (b) power exchange with the system (Adapted from [91]).

**Table 3.** Performance comparison of the system without virtual inertia (VI), simple virtual synchronous generator (VSG) based and adaptive dynamic programming (ADP) based VSG (Data from [91]).

Parameter	No VI	Simple VSG	ADP Based VSG
Peak Power for Event A	0 W	2184 W	1979 W
Settling time for Event A	12.6 s	35.1 s	31.3 s
Peak Power for Event B	0 W	−2235 W	−2029 W
Settling time for Event B	11.1 s	29.1 s	26.6 s
Energy delivered (Wh)	0 Wh	8.2 Wh	6.2 Wh
Net energy exchanged (Wh)	0 Wh	1.6 Wh	0.9 Wh

A similar online learning controller was proposed for virtual inertia implementation in a double fed induction generator (DFIG) based system in [87]. In this case, the controller was trained so as to restrict the frequency excursions to a minimum while maintaining the rotor speed of the DFIG within a safe operating range, rather than saving the energy flow from ESS. Other techniques to optimize the virtual inertia have been proposed in [88] using Linear-quadratic-regulator (LQR) and in [92] using fuzzy logic to minimize frequency deviations and ROCOF.

## 6. Challenges and Future Research Directions

### 6.1. Virtual Inertia as an Ancillary Service

Many research works have proposed the possibility of using virtual inertia as an ancillary service to improve frequency stability of large power grids. In [93], a control scheme to integrate DC microgrids as virtual inertia emulating units in the traditional AC grid has been presented. With the control scheme, the resources within the DC microgrid can be dispatched as an ancillary service for inertial response. Another major source of under-utilized energy lies in modern data centers. Data centers need a high degree of reliability, and as a result large amounts of backup energy storage which are unused during normal operating conditions. Research work in [94,95] have shown methods to utilize these resources using demand response techniques. This concept can be extended to use data center resources for virtual inertia implementation. Virtual inertia based interfaces, as mentioned in [93], can be integrated with data center resources for frequency regulation. A unit commitment model that combines system inertia from the conventional plants, and the virtual inertia from wind plants into system scheduling has been presented in [96], which allows for an economic analysis of the virtual inertia system.

Modern wind farms are already obligated through various laws and regulations to provide inertial ancillary services [97–100]. The uncaptured inertia in wind turbines, referred to as “hidden inertia”, can be captured through the techniques described in previous sections. Commercial wind turbine manufacturers, like WindINERTIA [101] and ENERCON [102], already provide virtual inertia response. Moreover, leading inverter manufacturers like FREQCON, Schneider Electric, and ABB already provide out-of-the-box inertial response capabilities. Using electric vehicles (EVs) to provide ancillary services has become a popular research topic [103]. Typically the control algorithm of the bidirectional converters in EVs can be modified for virtual inertia implementation [104,105].

### 6.2. Inertia Estimation

Research has been conducted in [106] to estimate the total inertia constant of the power system. The research was aimed at determining spinning reserve requirements for the power system. However, virtual inertia emulated using ESSs and RESs is not going to be constant as in the case of traditional synchronous generation. The available inertia in the system will depend upon whether RES units are online or not, and resource availability (wind speed, irradiance, and state of charge in case of ESS) [107]. System inertia estimation is thus going to be critical for planning purposes for system operators in the future power system with high RES penetrations. Furthermore, such estimates can provide helpful insights into the stable real-time operation of a power system. Inertia estimation using frequency transients measured using synchronized phasor measurement units (PMUs) was proposed in [107,108]. In [109], a method to estimate the inertial response of power system under high wind penetration based on the swing equation is presented. Accurate detection of frequency events and precise ROCOF measurements are critical for proper inertia estimation [110]. In the context of modern power systems with RES units participating in the inertial response, the inertia of the system will also largely depend on the RES resource availability at any given time as well. So, PV and wind forecasts data can be used to complement and further improve the inertia estimation techniques described before. Accurate inertia estimation methods will help setup a framework for system operator’s to procure inertial services.

### 6.3. Improved Modeling, Control and Aggregation of Virtual Inertia Systems

Most research has focused on specific implementations of virtual inertia and the broader impacts of inertial response. Current literature, lacks accurate, mathematical models which represent the dynamics of the system. Such models are essential for parameter tuning and understanding the operational behavior when virtual inertia systems are interconnected to the power system. In [75,111], a small-signal model for a virtual inertia system has been developed. The model was used to identify

critical operating modes through Eigenvalue analysis, and a technique to assess the sensitivity of the system to the parameter gains has been demonstrated. Similarly, a small-signal model of a synchronverter was developed in [32]. Such a model aids in improved tuning of the controller gains and provides granular control over how the overall system needs to be operated. An analytical approach to study the effect of microgrids with high RES penetration on the frequency stability has been described in [112]. Performance indices completely independent of the test system have also been proposed to better facilitate impact analysis. The behavior and coordination between virtual inertia systems and existing SGs are critical topics for further research. In the future, with numerous virtual inertia units, the coordinated and aggregated operation, and optimal placement will also be important research questions.

#### 6.4. Market Structure for Virtual Inertia Systems

Currently no market for virtual inertia nor for inertia from conventional SGs exists. SGs and some loads in the power system inherently provide inertial response and are treated as a free resource. As the power system becomes inverter-dominated, the inertial requirements will become a valuable tradeable commodity, and generating units will demand financial compensation. A market-based approach can be a cost effective solution to ensure sufficiency of inertial services in the future power market [113]. The inertial response can be provided by wind turbines or even PV systems with inherent storage technologies [114]. Schemes to operate PV systems below their MPP with reserve for inertial response is also a possible option with the suitable market for such resources. A scheme to trade inertia is presented in [11]. Furthermore, the paper argues inertia should not be traded in terms of power or energy, but rather in terms of an inertia metric. A unit commitment framework for fast frequency services in the power system with transient stability constraints representing the dynamic performance requirements was proposed in [115]. It was shown that additional inertia prevented expensive units being committed post-frequency event and reduced the overall system production cost in a power system. Other papers propose a penalty factor for generators that do not provide inertial response, but so far there is no clear structure on how the inertia market should operate and is an open research area.

One method that deserves further exploration is deploying inertia as “service” for power quality. For instance, as a microgrid operator, one can offer inertial services based on certain criteria such as maximum allowable ROCOFs and/or frequency deviation. The Quality of Service (QoS) metrics which have been proposed for cloud computing services (e.g., [116]) can be garnered for power systems to measure the power quality in terms on inertial response availability. The quality may be assessed in terms of response time after a frequency disturbance and/or inertia made available. This will foster a framework for microgrid operators to incorporate inertial response services in the system based on the requirements of its end-users.

#### 6.5. Energy Storage Resources for Virtual Inertia Systems

Typically, capacitors and batteries have been proposed as ESSs for dynamic frequency control using power electronic converters [45,50,72,82]. In [117], an ultra-capacitor based ESS is proposed to reduce the impact of RESs variability of frequency stability of an isolated power system. However, these energy resources often incorporate prohibitive cost investments, and because fast-frequency needs to be compensated by the virtual inertia systems it may effect the lifetime of the ESS. As a solution, a parallel combination of batteries and ultra-capacitors was proposed in [21] which significantly reduced the impact of high frequency dynamics on the batteries as the ultra-capacitors supplied the high frequency components. This also allowed for a cheaper and smaller battery unit [118]. Flywheel based energy storage for virtual inertia was proposed in [119]. Novel solar panel technologies with inherent storage capabilities could be another way of providing inertia through PV systems [114]. Recently, researchers have started to focus on alternate means of energy resource for virtual inertia. One of the main areas that is gaining attention is the so-called “thermal-inertia” of heating, ventilation,

and air conditioning (HVAC) systems of commercial buildings. As discussed in [120–122], the power consumption of the power electronics based HVAC units can be controlled to provide inertial response while ensuring that the customer comfort is not effected. Similarly, the large HVAC installation in data centers could be another potential to tap for inertial response in the future grid with large scale integration of RES units.

## 7. Conclusions

This paper presented a literature review of virtual inertia systems in the modern power system under high RES penetration. Numerous topologies for virtual inertia implementation, which constitutes the “first generation” of virtual inertia systems, were identified. It was shown that, fundamentally, the objective of all the topologies is to provide dynamic frequency response through power electronic converters. The appropriate topology can be selected based on the required architecture (current source or voltage source implementation) and desired level of sophistication in emulating the exact behavior of SGs. For example, for replication of the exact dynamics of SGs, topologies such as the synchronverter, VISMA and inducverters can be used. More simplistic topologies like Ise lab’s topology, SPC can be used if an approximate replication is sufficient. The VSG approach, on the other hand, is more suitable when the objective is to provide just the dynamic frequency response without emulating the exact behavior of SGs. An important takeaway through the literature review was that the droop based controllers, which were regarded as separate control method for inverter systems, are in fact fundamentally similar to virtual inertia systems as formalized by the literature pointed out.

Next, the second generation of virtual inertia systems with focus on optimization of existing virtual inertia topologies were reviewed. Such algorithms can prevent degradation of ESS lifetime and allow reduced curtailment of RES units that participate in inertial response. Furthermore, the enhancements help in improved dynamics and overall stability. Some of the challenges and possible areas where further research is required were also discussed. The current state-of-art of topics such as inertia estimation, improved controls and aggregation techniques, the virtual inertia market, and ESS for virtual inertia systems were also presented. This was followed by a discussion on possible research directions on these topics.

**Acknowledgments:** The authors would like to thank Microsoft Inc. and South Dakota Board of Regents (SDBOR) for the financial support. The authors are also thankful towards Mr. Jason Sternhagen for his help in proofreading the paper.

**Author Contributions:** Ujjwol Tamrakar replicated and analyzed the model of various topologies available in the literature; Ujjwol Tamrakar and Dipesh Shrestha developed one of the case studies; Ujjwol Tamrakar, Dipesh Shrestha, and Reinaldo Tonkoski analyzed the topologies and formulated the discussions in the manuscript. Ujjwol Tamrakar, Dipesh Shrestha, and Manisha Maharjan wrote the manuscript; Bishnu P. Bhattacharai and Timothy M. Hansen contributed on the formulation of the discussion and provided their comprehensive feedback on the paper.

**Conflicts of Interest:** The authors declare no conflict of interest.

## Abbreviations

The following abbreviations are used in this manuscript:

ADP	Adaptive Dynamic Programming
DFIG	Double Fed Induction Generator
DG	Distributed Generation
ENTSO-E	European Network of Transmission System Operators for Electricity
ERCOT	Electricity Reliability Council of Texas
ESS	Energy Storage System
HVAC	Heating, Ventilation and Air Conditioning
IEEE	Institute of Electrical and Electronic Engineers

IEPE	Institute of Electrical Power Engineering
LQR	Linear Quadratic Regulator
KHI	Kawasaki Heavy Industries
MPP	Maximum Power Point
NERC	North American Electric Reliability Corporation
PI	Proportional-Integral
PLL	Phase Locked Loop
PWM	Pulse Width Modulation
QoS	Quality of Service
RES	Renewable Energy System
ROCOF	Rate of Change of Frequency
SG	Synchronous Generator
SPC	Synchronous Power Controller
STATCOM	Static Synchronous Compensator
VI	Virtual Inertia
VISMA	Virtual Synchronous Machine
VOC	Virtual Oscillator Controller
VSG	Virtual Synchronous Generator
UFLS	Under Frequency Load Shedding

## References

1. U.S. Energy Information Administration. *Annual Energy Outlook 2017*; U.S. Department of Energy: Washington, DC, USA, 2017. Available online: [https://www.eia.gov/outlooks/aeo/pdf/0383\(2017\).pdf](https://www.eia.gov/outlooks/aeo/pdf/0383(2017).pdf) (accessed on 21 June 2017).
2. The Sunshot Initiative. Available online: <http://www.webcitation.org/6pV7YpHo2> (accessed on 5 April 2017).
3. IEA PVPS. *Trends in 2016 in Photovoltaic Applications*; T1-30:2016; IEA PVPS: Paris, France, 2016. Available online: [http://iea-pvps.org/fileadmin/dam/public/report/national/Trends\\_2016\\_-\\_mr.pdf](http://iea-pvps.org/fileadmin/dam/public/report/national/Trends_2016_-_mr.pdf) (accessed on 21 June 2017).
4. Kroposki, B.; Johnson, B.; Zhang, Y.; Gevorgian, V.; Denholm, P.; Hodge, B.M.; Hannegan, B. Achieving a 100% Renewable Grid: Operating Electric Power Systems with Extremely High Levels of Variable Renewable Energy. *IEEE Power Energy Mag.* **2017**, *15*, 61–73.
5. Hussein, M.M.; Senjyu, T.; Orabi, M.; Wahab, M.A.; Hamada, M.M. Control of a stand-alone variable speed wind energy supply system. *Appl. Sci.* **2013**, *3*, 437–456.
6. Yan, R.; Saha, T.K.; Modi, N.; Masood, N.A.; Mosadeghy, M. The combined effects of high penetration of wind and PV on power system frequency response. *Appl. Energy* **2015**, *145*, 320–330.
7. Electricity Reliability Council of Texas (ERCOT). *Future Ancillary Services in ERCOT*; ERCOT: Taylor, TX, USA, 2013. Available online: [http://www.ercot.com/content/news/presentations/2014/ERCOT\\_AS\\_Concept\\_Paper\\_Version\\_1.1\\_as\\_of\\_11-01-13\\_1445\\_black.pdf](http://www.ercot.com/content/news/presentations/2014/ERCOT_AS_Concept_Paper_Version_1.1_as_of_11-01-13_1445_black.pdf) (accessed on 21 June 2017).
8. Matevosyan, J.; Sharma, S.; Huang, S.H.; Woodfin, D.; Ragsdale, K.; Moorthy, S.; Wattles, P.; Li, W. Proposed future Ancillary Services in Electric Reliability Council of Texas. In Proceedings of the IEEE PowerTech, Eindhoven, The Netherlands, 29 June–2 July 2015; pp. 1–6.
9. Poolla, B.K.; Bolognani, S.; Dorfler, F. Optimal placement of virtual inertia in power grids. In Proceedings of the American Control Conference, Boston, MA, USA, 6–8 July 2016.
10. De Vyver, J.V.; Kooning, J.D.M.D.; Meersman, B.; Vandevelde, L.; Vandoorn, T.L. Droop Control as an Alternative Inertial Response Strategy for the Synthetic Inertia on Wind Turbines. *IEEE Trans. Power Syst.* **2016**, *31*, 1129–1138.
11. Thiesen, H.; Jauch, C.; Gloe, A. Design of a System Substituting Today's Inherent Inertia in the European Continental Synchronous Area. *Energies* **2016**, *9*, 582.
12. Gurung, A.; Galipeau, D.; Tonkoski, R.; Tamrakar, I. Feasibility study of Photovoltaic-hydropower microgrids. In Proceedings of the 5th International Conference on Power and Energy Systems (ICPS), Kathmandu, Nepal, 28–30 October 2014; pp. 1–6.

13. Tamrakar, U.; Galipeau, D.; Tonkoski, R.; Tamrakar, I. Improving transient stability of photovoltaic-hydro microgrids using virtual synchronous machines. In Proceedings of the IEEE Eindhoven PowerTech, Eindhoven, The Netherlands, 29 June–2 July 2015; pp. 1–6.
14. Guerrero, J.M.; de Vicuna, L.G.; Matas, J.; Castilla, M.; Miret, J. A wireless controller to enhance dynamic performance of parallel inverters in distributed generation systems. *IEEE Trans. Power Electron.* **2004**, *19*, 1205–1213.
15. Hatziaargyriou, N.; Asano, H.; Irvani, R.; Marnay, C. Microgrids. *IEEE Power Energy Mag.* **2007**, *5*, 78–94.
16. Kim, J.; Guerrero, J.M.; Rodriguez, P.; Teodorescu, R.; Nam, K. Mode Adaptive Droop Control With Virtual Output Impedances for an Inverter-Based Flexible AC Microgrid. *IEEE Trans. Power Electron.* **2011**, *26*, 689–701.
17. Under Frequency Load Shedding. Available online: <http://www.nerc.com/pa/RAPA/ri/Pages/UnderFrequencyLoadShedding.aspx> (accessed on 25 May 2017).
18. North American Electric Reliability Corporation (NERC). *Frequency Response Initiative Report: The Reliability Role of Frequency Response*; NERC: Atlanta, GA, USA, 2012. Available online: [http://www.nerc.com/docs/pc/FRI\\_Report\\_10-30-12\\_Master\\_w-appendices.pdf](http://www.nerc.com/docs/pc/FRI_Report_10-30-12_Master_w-appendices.pdf) (accessed on 21 June 2017).
19. Voltage Characteristics of Electricity Supplied by Public Distribution Systems. Available online: [http://www2.schneider-electric.com/library/SCHNEIDER\\_ELECTRIC/SE\\_LOCAL/APS/204836\\_1312/DraftStandard0026rev2-DraftEN501602005-05.pdf](http://www2.schneider-electric.com/library/SCHNEIDER_ELECTRIC/SE_LOCAL/APS/204836_1312/DraftStandard0026rev2-DraftEN501602005-05.pdf) (accessed on 21 June 2017).
20. ISO 8528-5:2005 Standard: Reciprocating Internal Combustion Engine Driven Alternating Current Generating Sets—Part 5: Generating Sets. 2005. Available online: <https://www.iso.org/standard/39047.html> (accessed on 21 June 2017).
21. Torres, M.; Lopes, L.A. Virtual synchronous generator: A control strategy to improve dynamic frequency control in autonomous power systems. *Energy Power Eng.* **2013**, *5*, 2A:1–2A:7. Available online: [http://file.scirp.org/Html/5-6201497\\_30602.htm](http://file.scirp.org/Html/5-6201497_30602.htm) (accessed on 29 April 2017).
22. Shrestha, D.; Tamrakar, U.; Ni, Z.; Tonkoski, R. Experimental Verification of Virtual Inertia in Diesel Generator based Microgrids. In Proceedings of the 18th Annual International Conference on Industrial Technology (ICIT), Toronto, ON, Canada, 22–25 March 2017; pp. 95–100.
23. Rahmann, C.; Castillo, A. Fast Frequency Response Capability of Photovoltaic Power Plants: The Necessity of New Grid Requirements and Definitions. *Energies* **2014**, *7*, 6306–6322.
24. Chang-Chien, L.R.; Lin, W.T.; Yin, Y.C. Enhancing Frequency Response Control by DFIGs in the High Wind Penetrated Power Systems. *IEEE Trans. Power Syst.* **2011**, *26*, 710–718.
25. Tielens, P.; Hertem, D.V. The relevance of inertia in power systems. *Renew. Sustain. Energy Rev.* **2016**, *55*, 999–1009.
26. Beck, H.P.; Hesse, R. Virtual synchronous machine. In Proceedings of the 9th International Conference on Electrical Power Quality and Utilisation, Barcelona, Spain, 9–11 October 2007; pp. 1–6.
27. Gonzalez-Longatt, F.; Chikuni, E.; Rashayi, E. Effects of the Synthetic Inertia from wind power on the total system inertia after a frequency disturbance. In Proceedings of the IEEE International Conference on Industrial Technology (ICIT), Cape Town, South Africa, 25–28 February 2013; pp. 826–832.
28. Bevrani, H.; Ise, T.; Miura, Y. Virtual synchronous generators: A survey and new perspectives. *Int. J. Electr. Power Energy Syst.* **2014**, *54*, 244–254.
29. Zhong, Q.C.; Weiss, G. Synchronverters: Inverters That Mimic Synchronous Generators. *IEEE Trans. Ind. Electron.* **2011**, *58*, 1259–1267.
30. Zhong, Q.C. Virtual Synchronous Machines: A unified interface for grid integration. *IEEE Power Electron. Mag.* **2016**, *3*, 18–27.
31. Kundur, P.; Balu, N.J.; Lauby, M.G. *Power System Stability and Control*; McGraw-Hill: New York, NY, USA, 1994.
32. Piya, P.; Karimi-Ghartemani, M. A stability analysis and efficiency improvement of synchronverter. In Proceedings of the IEEE Applied Power Electronics Conference and Exposition (APEC), Long Beach, CA, USA, 20–24 March 2016; pp. 3165–3171.
33. Zhong, Q.C.; Hornik, T. Sinusoid-Locked Loops. In *Control of Power Inverters in Renewable Energy and Smart Grid Integration*; John Wiley & Sons, Ltd.: Hoboken, NJ, USA, 2012; pp. 379–392.

34. Ferreira, R.V.; Silva, S.M.; Brandao, D.I.; Antunes, H.M.A. Single-phase synchronverter for residential PV power systems. In Proceedings of the 17th International Conference on Harmonics and Quality of Power (ICHQP), Belo Horizonte, Brazil, 16–19 October 2016; pp. 861–866.
35. Shinnaka, S. A Robust Single-Phase PLL System With Stable and Fast Tracking. *IEEE Trans. Ind. Appl.* **2008**, *44*, 624–633.
36. Zhang, L.; Harnefors, L.; Nee, H.P. Power-Synchronization Control of Grid-Connected Voltage-Source Converters. *IEEE Trans. Power Syst.* **2010**, *25*, 809–820.
37. Wang, S.; Hu, J.; Yuan, X. Virtual Synchronous Control for Grid-Connected DFIG-Based Wind Turbines. *IEEE J. Emerg. Sel. Top. Power Electron.* **2015**, *3*, 932–944.
38. Zhong, Q.C.; Nguyen, P.L.; Ma, Z.; Sheng, W. Self-Synchronized Synchronverters: Inverters Without a Dedicated Synchronization Unit. *IEEE Trans. Power Electron.* **2014**, *29*, 617–630.
39. Ma, Z.; Zhong, Q.C.; Yan, J.D. Synchronverter-based control strategies for three-phase PWM rectifiers. In Proceedings of the 7th IEEE Conference on Industrial Electronics and Applications (ICIEA), Singapore, 18–20 July 2012; pp. 225–230.
40. Sakimoto, K.; Miura, Y.; Ise, T. Stabilization of a power system with a distributed generator by a Virtual Synchronous Generator function. In Proceedings of the 8th International Conference on Power Electronics (ECCE Asia), Jeju, Korea, 30 May–3 June 2011; pp. 1498–1505.
41. Alipoor, J.; Miura, Y.; Ise, T. Power System Stabilization Using Virtual Synchronous Generator With Alternating Moment of Inertia. *IEEE J. Emerg. Sel. Top. Power Electron.* **2015**, *3*, 451–458.
42. Liu, J.; Miura, Y.; Ise, T. Dynamic characteristics and stability comparisons between virtual synchronous generator and droop control in inverter-based distributed generators. In Proceedings of the International Power Electronics Conference (IPEC-Hiroshima 2014-ECCE ASIA), Hiroshima, Japan, 18–21 May 2014; pp. 1536–1543.
43. Sakimoto, K.; Miura, Y.; Ise, T. Characteristics of Parallel Operation of Inverter-Type Distributed Generators Operated by a Virtual Synchronous Generator. *Electr. Eng. Jpn.* **2015**, *192*, 9–19.
44. Torres, M.; Lopes, L.A.C. Virtual synchronous generator control in autonomous wind-diesel power systems. In Proceedings of the IEEE Electrical Power & Energy Conference (EPEC), Montreal, QC, Canada, 22–23 October 2009; pp. 1–6.
45. Van Wesenbeeck, M.P.N.; de Haan, S.W.H.; Varela, P.; Visscher, K. Grid tied converter with virtual kinetic storage. In Proceedings of the IEEE Bucharest PowerTech, Bucharest, Romania, 28 June–2 July 2009; pp. 1–7.
46. Van, T.V.; Visscher, K.; Diaz, J.; Karapanos, V.; Woyte, A.; Albu, M.; Bozelie, J.; Loix, T.; Federenciu, D. Virtual synchronous generator: An element of future grids. In Proceedings of the IEEE Innovative Smart Grid Technologies Conference Europe (ISGT Europe), Gothenberg, Sweden, 11–13 October 2010; pp. 1–7.
47. Wen, B.; Boroyevich, D.; Burgos, R.; Mattavelli, P.; Shen, Z. Small-Signal Stability Analysis of Three-Phase AC Systems in the Presence of Constant Power Loads Based on Measured d-q Frame Impedances. *IEEE Trans. Power Electron.* **2015**, *30*, 5952–5963.
48. Tamrakar, U.; Tonkoski, R.; Ni, Z.; Hansen, T.M.; Tamrakar, I. Current control techniques for applications in virtual synchronous machines. In Proceedings of the 6th IEEE International Conference on Power Systems (ICPS), New Delhi, India, 4–6 March 2016; pp. 1–6.
49. Malesani, L.; Tomasin, P. PWM current control techniques of voltage source converters—A survey. In Proceedings of the International Conference on Industrial Electronics, Control, and Instrumentation (IECON '93), Maui, HI, USA, 15–19 November 1993; pp. 670–675.
50. Driesen, J.; Visscher, K. Virtual synchronous generators. In Proceedings of the 9th IEEE Power & Energy Society General Meeting, Pittsburgh, PA, USA, 20–24 July 2008; pp. 1–6.
51. Karapanos, V.; de Haan, S.; Zwetsloot, K. Real time simulation of a power system with VSG hardware in the loop. In Proceedings of the 37th Annual Conference of the IEEE Industrial Electronics Society (IECON), Melbourne, Australia, 7–10 November 2011; pp. 3748–3754.
52. Thong, V.V.; Woyte, A.; Albu, M.; Hest, M.V.; Bozelie, J.; Diaz, J.; Loix, T.; Stanculescu, D.; Visscher, K. Virtual synchronous generator: Laboratory scale results and field demonstration. In Proceedings of the IEEE Bucharest PowerTech, Bucharest, Romania, 28 June–2 July 2009; pp. 1–6.
53. Morren, J.; Pierik, J.; de Haan, S.W. Inertial response of variable speed wind turbines. *Electr. Power Syst. Res.* **2006**, *76*, 980–987.

54. Arani, M.F.M.; El-Saadany, E.F. Implementing Virtual Inertia in DFIG-Based Wind Power Generation. *IEEE Trans. Power Syst.* **2013**, *28*, 1373–1384.
55. Zhang, W.; Cantarellas, A.M.; Rocabert, J.; Luna, A.; Rodriguez, P. Synchronous Power Controller With Flexible Droop Characteristics for Renewable Power Generation Systems. *IEEE Trans. Sustain. Energy* **2016**, *7*, 1572–1582.
56. Blaabjerg, F.; Teodorescu, R.; Liserre, M.; Timbus, A.V. Overview of Control and Grid Synchronization for Distributed Power Generation Systems. *IEEE Trans. Ind. Electron.* **2006**, *53*, 1398–1409.
57. European Network of Transmission System Operators for Electricity (ENTSO-E). *Need for Synthetic Inertia (SI) for Frequency Regulation*; ENTSO-E: Brussels, Belgium, 2017. Available online: [https://consultations.entsoe.eu/system-development/entso-e-connection-codes-implementation-guidance-d-3/user\\_uploads/igd-need-for-synthetic-inertia.pdf](https://consultations.entsoe.eu/system-development/entso-e-connection-codes-implementation-guidance-d-3/user_uploads/igd-need-for-synthetic-inertia.pdf) (accessed on 21 June 2017).
58. Ashabani, M.; Freijedo, F.D.; Golestan, S.; Guerrero, J.M. Inducverters: PLL-Less Converters With Auto-Synchronization and Emulated Inertia Capability. *IEEE Trans. Smart Grid* **2016**, *7*, 1660–1674.
59. D'Arco, S.; Suul, J.A. Virtual synchronous machines- Classification of implementations and analysis of equivalence to droop controllers for microgrids. In Proceedings of the IEEE Grenoble Conference, Grenoble, France, 16–20 June 2013; pp. 1–7.
60. Midtsund, T.; Suul, J.A.; Undeland, T. Evaluation of current controller performance and stability for voltage source converters connected to a weak grid. In Proceedings of the IEEE 2nd International Symposium on Power Electronics for Distributed Generation Systems, Hefei, China, 16–18 June 2010; pp. 382–388.
61. Svensson, J. Synchronisation methods for grid-connected voltage source converters. *IEE Proc. Gener. Transm. Distrib.* **2001**, *148*, 229–235.
62. Katiraei, F.; Iravani, M.R. Power Management Strategies for a Microgrid With Multiple Distributed Generation Units. *IEEE Trans. Power Syst.* **2006**, *21*, 1821–1831.
63. Pogaku, N.; Prodanovic, M.; Green, T.C. Modeling, Analysis and Testing of Autonomous Operation of an Inverter-Based Microgrid. *IEEE Trans. Power Electron.* **2007**, *22*, 613–625.
64. D'Arco, S.; Suul, J.A. Equivalence of Virtual Synchronous Machines and Frequency-Droops for Converter-Based MicroGrids. *IEEE Trans. Smart Grid* **2014**, *5*, 394–395.
65. Li, C.; Burgos, R.; Cvetkovic, I.; Boroyevich, D.; Mili, L.; Rodriguez, P. Analysis and design of virtual synchronous machine based STATCOM controller. In Proceedings of the IEEE 15th Workshop on Control and Modeling for Power Electronics (COMPEL), Santander, Spain, 22–25 June 2014; pp. 1–6.
66. Soni, N.; Doolla, S.; Chandorkar, M.C. Improvement of Transient Response in Microgrids Using Virtual Inertia. *IEEE Trans. Power Deliv.* **2013**, *28*, 1830–1838.
67. Hesse, R.; Turschner, D.; Beck, H.P. Micro grid stabilization using the Virtual Synchronous Machine (VISMA). In Proceedings of the International Conference on Renewable Energies and Power Quality, ICREPQ'09, Valencia, Spain, 15–17 April 2009; pp. 1–6.
68. Virtual Synchronous Machine. Available online: <https://fenix.tecnico.ulisboa.pt/downloadFile/395145918861/paper.pdf> (accessed on 17 June 2017).
69. Chen, Y.; Hesse, R.; Turschner, D.; Beck, H.P. Dynamic properties of the virtual synchronous machine (VISMA). In Proceedings of the International Conference on Renewable Energies and Power Quality, Las Palmas de Gran Canaria, Spain, 13–15 April 2011; pp. 1–5.
70. Chen, Y.; Hesse, R.; Turschner, D.; Beck, H.P. Comparison of methods for implementing virtual synchronous machine on inverters. In Proceedings of the International Conference on Renewable Energies and Power Quality, Santiago de Compostela, Spain, 28–30 March 2012; pp. 1–6.
71. Hirase, Y.; Abe, K.; Sugimoto, K.; Shindo, Y. A grid connected inverter with virtual synchronous generator model of algebraic type. *IEEE Trans. Power Energy* **2012**, *132*, 371–380.
72. Rodriguez, P.; Candela, I.; Luna, A. Control of PV generation systems using the synchronous power controller. In Proceedings of the IEEE Energy Conversion Congress and Exposition (ECCE), Denver, CO, USA, 15–19 September 2013; pp. 993–998.
73. Rodriguez, C.; Candela, G.; Rocabert, D.; Teodorescu, R. Virtual Controller of Electromechanical Characteristics for Static Power Converters. U.S. Patent US20140067138 A1, 27 February 2012.
74. Cortés, P.; Garcia, J.; Delgado, J.; Teodorescu, R. Virtual Admittance Controller Based on Static Power Converters. U.S. Patent US20140049233 A1, 20 February 2014.

75. D'Arco, S.; Suul, J.A.; Fosso, O.B. Control system tuning and stability analysis of Virtual Synchronous Machines. In Proceedings of the IEEE Energy Conversion Congress and Exposition (ECCE), Denver, CO, USA, 15–19 September 2013; pp. 2664–2671.
76. Zhang, W.; Remon, D.; Mir, A.; Luna, A.; Rocabert, J.; Candela, I.; Rodriguez, P. Comparison of different power loop controllers for synchronous power controlled grid-interactive converters. In Proceedings of the IEEE Energy Conversion Congress and Exposition (ECCE), Montreal, QC, Canada, 20–24 September 2015; pp. 3780–3787.
77. Behera, R.R.; Thakur, A.N. An overview of various grid synchronization techniques for single-phase grid integration of renewable distributed power generation systems. In Proceedings of the International Conference on Electrical, Electronics, and Optimization Techniques (ICEEOT), Chennai, India, 3–5 March 2016; pp. 2876–2880.
78. Johnson, B.B.; Dhople, S.V.; Hamadeh, A.O.; Krein, P.T. Synchronization of Parallel Single-Phase Inverters With Virtual Oscillator Control. *IEEE Trans. Power Electron.* **2014**, *29*, 6124–6138.
79. Johnson, B.B.; Dhople, S.V.; Cale, J.L.; Hamadeh, A.O.; Krein, P.T. Oscillator-Based Inverter Control for Islanded Three-Phase Microgrids. *IEEE J. Photovolt.* **2014**, *4*, 387–395.
80. Dhople, S.V.; Johnson, B.B.; Hamadeh, A.O. Virtual Oscillator Control for voltage source inverters. In Proceedings of the 51st Annual Allerton Conference on Communication, Control, and Computing (Allerton), Monticello, IL, USA, 2–4 October 2013; pp. 1359–1363.
81. Zhang, C.H.; Zhong, Q.C.; Meng, J.S.; Chen, X.; Huang, Q.; Chen, S.H.; Lv, Z.P. An improved synchronverter model and its dynamic behaviour comparison with synchronous generator. In Proceedings of the 2nd IET Renewable Power Generation Conference (RPG), Beijing, China, 9–11 September 2013; pp. 1–4.
82. Natarajan, V.; Weiss, G. Synchronverters with better stability due to virtual inductors, virtual capacitors and anti-windup. *IEEE Trans. Ind. Electron.* **2017**, *64*, 5994–6004.
83. Dong, S.; Chen, Y.C. Adjusting Synchronverter Dynamic Response Speed via Damping Correction Loop. *IEEE Trans. Energy Convers.* **2017**, *32*, 608–619.
84. Zhong, Q.C.; Konstantopoulos, G.C.; Ren, B.; Krstic, M. Improved Synchronverters with Bounded Frequency and Voltage for Smart Grid Integration. *IEEE Trans. Smart Grid* **2017**, doi:10.1109/TSG.2016.2565663.
85. Liu, J.; Miura, Y.; Bevrani, H.; Ise, T. Enhanced Virtual Synchronous Generator Control for Parallel Inverters in Microgrids. *IEEE Trans. Smart Grid* **2016**, doi:10.1109/TSG.2016.2521405.
86. Alipoor, J.; Miura, Y.; Ise, T. Stability Assessment and Optimization Methods for Microgrid with Multiple VSG Units. *IEEE Trans. Smart Grid* **2016**, doi:10.1109/TSG.2016.2592508.
87. Guo, W.; Liu, F.; Si, J.; Mei, S. Incorporating approximate dynamic programming-based parameter tuning into PD-type virtual inertia control of DFIGs. In Proceedings of the International Joint Conference on Neural Networks (IJCNN), Dallas, TX, USA, 4–9 August 2013; pp. 1–8.
88. Torres, M.; Lopes, L.A. An optimal virtual inertia controller to support frequency regulation in autonomous diesel power systems with high penetration of renewables. In Proceedings of the International Conference on Renewable Energies and Power Quality (ICREPQ 11), la Palmas de Gran Canaria, Spain, 13–15 April 2011; pp. 1–6.
89. Torres L., M.A.; Lopes, L.A.C.; Morán T., L.A.; Espinoza C., J.R. Self-Tuning Virtual Synchronous Machine: A Control Strategy for Energy Storage Systems to Support Dynamic Frequency Control. *IEEE Trans. Energy Convers.* **2014**, *29*, 833–840.
90. Shrestha, D.; Tamrakar, U.; Malla, N.; Ni, Z.; Tonkoski, R. Reduction of energy consumption of virtual synchronous machine using supplementary adaptive dynamic programming. In Proceedings of the IEEE International Conference on Electro Information Technology (EIT), Grand Forks, ND, USA, 19–21 May 2016; pp. 690–694.
91. Shrestha, D. Virtual Inertia Emulation to Improve Dynamic Frequency Stability of Low Inertia Microgrids. Master of Science thesis, South Dakota State University, Brookings, SD, USA, 2016.
92. Datta, M.; Ishikawa, H.; Naitoh, H.; Senjyu, T. Frequency control improvement in a PV-diesel hybrid power system with a virtual inertia controller. In Proceedings of the 7th IEEE Conference on Industrial Electronics and Applications (ICIEA), Singapore, 18–20 July 2012; pp. 1167–1172.
93. Chen, D.; Xu, Y.; Huang, A.Q. Integration of DC Microgrids as Virtual Synchronous Machines into the AC Grid. *IEEE Trans. Ind. Electron.* **2017**, doi:10.1109/TIE.2017.267462.

94. Bajracharya, L.; Awasthi, S.; Chalise, S.; Hansen, T.M.; Tonkoski, R. Economic analysis of a data center virtual power plant participating in demand response. In Proceedings of the IEEE Power and Energy Society General Meeting (PESGM), Boston, MA, USA, 17–21 July 2016; pp. 1–5.
95. Awasthi, S.R.; Chalise, S.; Tonkoski, R. Operation of datacenter as virtual power plant. In Proceedings of the IEEE Energy Conversion Congress and Exposition (ECCE), Montreal, QC, Canada, 20–24 September 2015; pp. 3422–3429.
96. Teng, F.; Strbac, G. Evaluation of synthetic inertia provision from wind plants. In Proceedings of the IEEE Power & Energy Society General Meeting, Denver, CO, USA, 26–30 July 2015; pp. 1–5.
97. Bousseau, P.; Belhomme, R.; Monnot, E.; Laverdure, N.; Boëda, D.; Roye, D.; Bacha, S. Contribution of wind farms to ancillary services. *Cigre* **2006**, *21*, 1–11.
98. Van Thong, V.; Driesen, J.; Belmans, R. Using Distributed Generation to Support and Provide Ancillary Services for the Power System. In Proceedings of the International Conference on Clean Electrical Power, Capri, Italy, 21–23 May 2007; pp. 159–163.
99. Teninge, A.; Jecu, C.; Roye, D.; Bacha, S.; Duval, J.; Belhomme, R. Contribution to frequency control through wind turbine inertial energy storage. *IET Renew. Power Gen.* **2009**, *3*, 358–370.
100. Yingcheng, X.; Nengling, T. Review of contribution to frequency control through variable speed wind turbine. *Renew. Energy* **2011**, *36*, 1671–1677.
101. Yan, R.; Saha, T.K. Frequency response estimation method for high wind penetration considering wind turbine frequency support functions. *IET Renew. Power Gen.* **2015**, *9*, 775–782.
102. Can Synthetic Inertia from Wind Power Stabilize Grids? Available online: <http://www.webcitation.org/6pscLoEBs> (accessed on 20 April 2017).
103. Kempton, W.; Tomić, J. Vehicle-to-grid power fundamentals: Calculating capacity and net revenue. *J. Power Sources* **2005**, *144*, 268–279.
104. Almeida, P.R.; Soares, F.; Lopes, J.P. Electric vehicles contribution for frequency control with inertial emulation. *Electr. Power Syst. Res.* **2015**, *127*, 141–150.
105. Meng, J.; Mu, Y.; Wu, J.; Jia, H.; Dai, Q.; Yu, X. Dynamic frequency response from electric vehicles in the Great Britain power system. *J. Mod. Power Syst. Clean Energy* **2015**, *3*, 203–211.
106. Inoue, T.; Taniguchi, H.; Ikeguchi, Y.; Yoshida, K. Estimation of power system inertia constant and capacity of spinning-reserve support generators using measured frequency transients. *IEEE Trans. Power Syst.* **1997**, *12*, 136–143.
107. Zhang, Y.; Bank, J.; Wan, Y.H.; Muljadi, E.; Corbus, D. Synchrophasor Measurement-Based Wind Plant Inertia Estimation. In Proceedings of the IEEE Green Technologies Conference (GreenTech), Denver, CO, USA, 4–5 April 2013; pp. 494–499.
108. Ashton, P.M.; Saunders, C.S.; Taylor, G.A.; Carter, A.M.; Bradley, M.E. Inertia Estimation of the GB Power System Using Synchrophasor Measurements. *IEEE Trans. Power Syst.* **2015**, *30*, 701–709.
109. Lara-Jimenez, J.D.; Ramirez, J.M. Inertial frequency response estimation in a power system with high wind energy penetration. In Proceedings of the IEEE Eindhoven PowerTech, Eindhoven, The Netherlands, 29 June–2 July 2015; pp. 1–6.
110. Wall, P.; Regulski, P.; Rusidovic, Z.; Terzija, V. Inertia estimation using PMUs in a laboratory. In Proceedings of the IEEE Power & Energy Society Innovative Smart Grid Technologies (ISTG-Europe), Istanbul, Turkey, 12–15 October 2014; pp. 1–6.
111. D’Arco, S.; Suul, J.A.; Fosso, O.B. Small-signal modeling and parametric sensitivity of a virtual synchronous machine in islanded operation. *Int. J. Electr. Power Energy Syst.* **2015**, *72*, 3–15.
112. Golpîra, H.; Seifi, H.; Messina, A.R.; Haghifam, M.R. Maximum Penetration Level of Micro-Grids in Large-Scale Power Systems: Frequency Stability Viewpoint. *IEEE Trans. Power Syst.* **2016**, *31*, 5163–5171.
113. Agranat, O.; MacGill, I.; Bruce, A. Fast Frequency Markets under High Penetrations of Renewable Energy in the Australian National Electricity Market. In Proceedings of the Asia-Pacific Solar Research Conference, Queensland, Australia, 8–10 December 2015.
114. Gurung, A.; Chen, K.; Khan, R.; Abdulkarim, S.S.; Varnekar, G.; Pathak, R.; Naderi, R.; Qiao, Q. Highly Efficient Perovskite Solar Cell Photocharging of Lithium Ion Battery Using DC–DC Booster. *Adv. Energy Mater.* **2017**. doi:10.1002/aenm.201602105.

115. Xu, T.; Jang, W.; Overbye, T. An Economic Evaluation Tool of Inertia Services for Systems with Integrated Wind Power and Fast-Acting Storage Resources. In Proceedings of the 49th Hawaii International Conference on System Sciences (HICSS), Hostelling International, Koloa, HI, USA, 5–8 January 2016; pp. 2456–2465.
116. Garg, S.K.; Versteeg, S.; Buyya, R. A framework for ranking of cloud computing services. *Future Gen. Comput. Syst.* **2013**, *29*, 1012–1023.
117. Delille, G.; François, B.; Malarange, G. Dynamic frequency control support: A virtual inertia provided by distributed energy storage to isolated power systems. In Proceedings of the 2010 IEEE PES Innovative Smart Grid Technologies Conference Europe (ISGT Europe), Gothenberg, Sweden, 18 November 2010; pp. 1–8.
118. Baisden, A.C.; Emadi, A. ADVISOR-based model of a battery and an ultra-capacitor energy source for hybrid electric vehicles. *IEEE Trans. Veh. Technol.* **2004**, *53*, 199–205.
119. Pena-Alzola, R.; Campos-Gaona, D.; Ordonez, M. Control of flywheel energy storage systems as virtual synchronous machines for microgrids. In the Proceedings of the IEEE 16th Workshop on Control and Modeling for Power Electronics (COMPEL), Vancouver, BC, Canada, 12–15 July 2015; pp. 1–7.
120. Hao, H.; Lin, Y.; Kowli, A.S.; Barooah, P.; Meyn, S. Ancillary Service to the Grid Through Control of Fans in Commercial Building HVAC Systems. *IEEE Trans. Smart Grid* **2014**, *5*, 2066–2074.
121. Beil, I.; Hiskens, I.; Backhaus, S. Frequency Regulation From Commercial Building HVAC Demand Response. *Proc. IEEE* **2016**, *104*, 745–757.
122. Cao, Y.; Magerko, J.A.; Navidi, T.; Krein, P.T. Power Electronics Implementation of Dynamic Thermal Inertia to Offset Stochastic Solar Resources in Low-Energy Buildings. *IEEE J. Emerg. Sel. Top. Power Electron.* **2016**, *4*, 1430–1441.



© 2017 by the authors. Licensee MDPI, Basel, Switzerland. This article is an open access article distributed under the terms and conditions of the Creative Commons Attribution (CC BY) license (<http://creativecommons.org/licenses/by/4.0/>).